THERMOGRAPHY FOR CHARACTERIZATION OF CORROSION DAMAGE

Ignacio Perez and Paul Kulowitch
Naval Air Warfare Center, Aircraft Division
Patuxent River MD 20670

ABSTRACT

Thermography is a viable NDE technique for the characterization of corrosion in metallic materials. Thermography is a rapid, non-contact, wide area inspection technique that is easy to interpret and that in not significantly sensitive to material curvature. We have developed a portable system and have characterized the sensitivity of the technique. Results will be presented in this paper.

Keywords: Thermography, thermographic inspection, corrosion, naval aviation, corrosive environment, lateral heat effects.

INTRODUCTION

The Navy operates in the most corrosive environment of any of the DoD services or commercial aviation. As a result corrosion prevention, detection and repair are of outmost importance to the Navy. All the materials in our platform are designed and engineered to offer the maximum corrosion protection without limiting their structural characteristics. New paint systems are being developed that comply with EPA regulations while providing enhanced protection against the environment. No matter how much protection we provide to our platforms in the form of improved materials, sealants and paints, the environment ultimately will penetrate the coating and initiate corrosion. This process can be exacerbated or mitigated by the specific mission of the platform. Low flying antisubmarine aircraft will corrode at an accelerated rate when compared to high-altitude communications aircraft.

The cost of corrosion control is enormous and accelerating as our fleet ages. This is especially significant in today's environment of reduced budgets and decreasing personnel. With fewer new acquisitions, the Navy is increasingly being forced to extend the life of existing platforms beyond their original design life to meet mission requirements. In order to maintain fleet readiness and safety, improved inspection methods are required that can detect the occurrence of corrosion quickly and reliably.

New techniques are being developed at the Naval Air Warfare Center aimed at the reliable and rapid inspection of corrosion in Naval aircraft. One of such techniques is pulsed thermography. This is a wide area inspection technique which is especially suited for the detection of hidden corrosion. It requires no contact media to perform the inspection as opposed to more conventional techniques such as ultrasonic inspection. This technique relies on the thermal gradients that result from
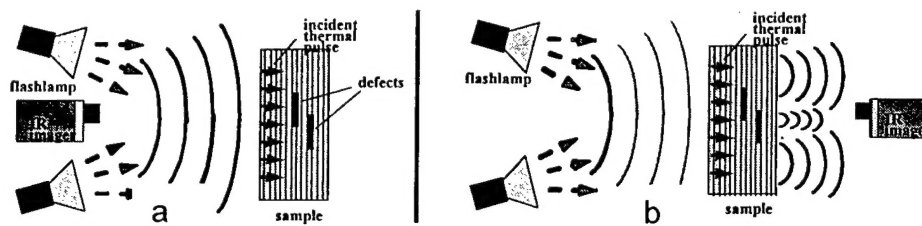
Figure 1. (a) Shows a standard single side inspection setup with the IR camera and the arc lamps in the same side. (b) Shows a through transmission setup which in general provides twice the depth of resolution.

the interaction between the thermal fields and defects present in the structure. This technique is also significantly insensitive to curvature and is a relatively easy interpretation method.

EXPERIMENTAL

The minimum number of experimental components needed to perform pulsed thermography are a heat source and an infrared (IR) camera. The proper choice of heat source is paramount for a successful thermographic experiment. Such source must be chosen so as to maximize the thermal contrast between the defect and the surrounding material. In some cases one can maximize the thermal contrast by heating the defect exclusively without disrupting the surrounding material such as when using microwave energy for detecting water entrapped inside a ceramic material. The microwave energy will propagate through the ceramic material without heating it and finally will be absorbed by any water present in it. This approach is not always possible and one has to resort to exploiting other defect properties (such as geometrical features) to enhance the thermal contrast. The most common energy sources used to thermally excite materials are: air heat guns, microwave sources, infrared lamps and arc lamps. All the samples studied in this paper were thermally excited using a pair of xenon arc lamps, each one powered by a 5 KJoule capacitor bank with a 10 msec discharge time. The IR camera used in these experiments was a Amber Engineering InSb focal plane array (128 x 128) camera with silicon optics operating in the 3 - 5 micron spectral range. Figure 1a (single side inspection setup) shows the experimental configuration used to image all defects. Other experimental arrangements are possible such as the one shown on Fig. 1b (through transmission setup). This setup is not well suited for field inspections where only one side is typically exposed, but has twice the depth of resolution than single side inspection methods. Figure 2 shows the camera system and arc lamps used to acquire data for this paper.

Any material can be inspected thermographically (such as metals, ceramics and composites) but the outcome of the inspection will depend on many factors such as sample geometry, sample thickness, amount of heat used, surface emissivity, specific heat, material density, thermal conductivity, defect depth and the size of the defect and other parameters. To gain insight into the effect that several of these parameters have on the thermographic process we fabricated various aluminum 7075 T6 panels with embedded defects. One panel was fabricated with flat bottom holes while the others had water pockets on the back. Figure 3 shows two thermal images a few msec after exposure to a heat pulse. The figure on the left corresponds to a t_o=1/8" thick aluminum panel with three different radii flat bottom holes (R=1/2", 3/8" and 1/4" diameter).
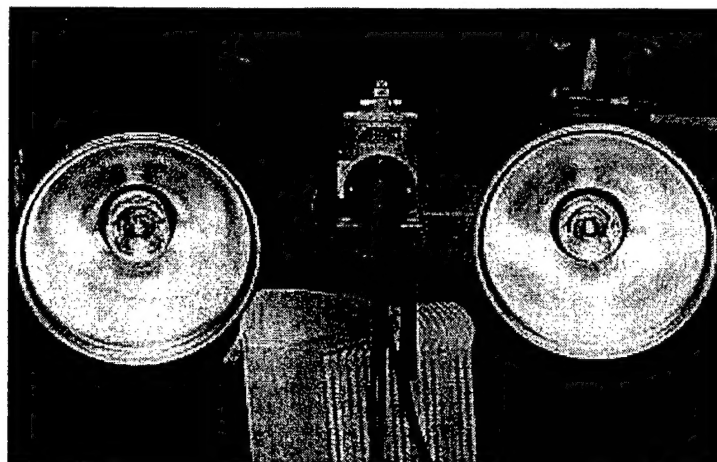

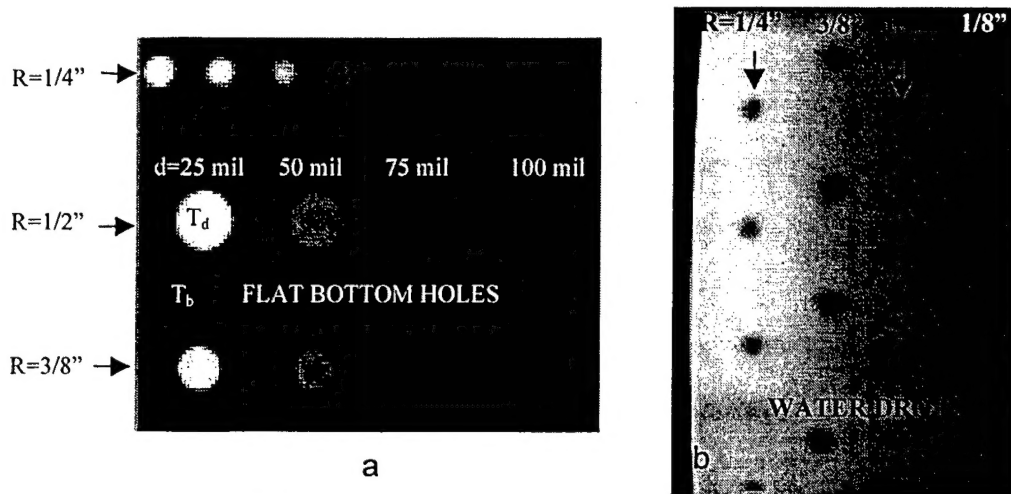Figure 2: Thermal imaging system used to acquire data.

Figure 3. (a) Shows a 1/8" thick aluminum with flat bottom holes of different depth ranging from 25 mil to 100 mil and three different radii of R=1/2",3/8" and 1/4". (b) Shows a 1/32" thick aluminum panel with water drops of different radii and different water content.

Flat bottom holes are a crude simulation to material loss that results from the corrosion process, but offer a simple means of generating standards for the characterization of the thermal process. The distance from the surface of the panel to the surface of the flat bottom holes (also referred as the defect depth "d") ranged from 25 mil to 100 mil. The largest contrast corresponds to the defect closest to the surface while the defect furthest from the surface showed the smallest thermal contrast. The thermal contrast is defined as the difference of the temperature above the defect (T_d on fig 3 a) from the temperature of a point away from the defect area (such as T_b on Fig. 3). The center to center distance between flat bottom holes was set to at least 2 diameters to minimize inter-hole proximity effects.

Water entrapment is a leading cause of corrosion and debonding in honeycomb structures. Early detection of it leads to economical repairs. Figure 3 b shows the thermal image a few msec after exposure of one of three panels (panel thickness were t_o=1/32", 1/16" and 1/8") fabricated to model water entrapment. The panel shown on that figure corresponds to a t_o=1/32" thick aluminum panel with water drops on the back of different diameters (1/8", 1/4", 3/8"and 1/2" diameter) and with different amount of water in them. Water was contained on the back of the panels by gluing straws of different diameters to the surface and by filling them with water up to different levels. The heights of water used were d = 1/16", 1/8", 3/16" and 1/4". It is clear from Figure 3b that the amount of water has little effect on the thermal contrast (notice the small contrast variation among drops of equal radii). The straws were staggered to maximize the spacing among them in order to minimize proximity effects. It is interesting to note the opposite nature of the thermal contrast effects when imaging flat bottom holes compared to when detecting water entrapment. When imaging flat bottom holes it is the thinner region above the defect what ultimately makes this region appear hotter (white region on Figure 3a). In contrast, it is the excess water acting as a heat sink what makes the region above the entrapped water appear colder (black region on Figure 3b).

RESULTS AND INTERPRETATION

Figure 4 shows the contrast data of all the samples studied, the graph on the left corresponds to flat bottom hole samples while the graph on the right corresponds to samples with water pockets on the back. From the graph 4a clear that the deeper the defect (or the smaller amount of mass loss) the smaller the contrast temperature will be. Also, as the diameter of the defect gets smaller the contrast temperature diminishes. These results have been previously explained[1,2] using a simple lateral heat approximation model. The main result of the model is that the contrast temperature of a sample with a defect can be approximated by

$$\Delta T_{contrast} = \frac{Q}{\rho c}\left(\frac{1}{d} - \frac{1}{t_o}\right) \cdot \left[\frac{R}{2}\frac{t_o}{d(t_o - d)}\right]^{\frac{1}{1 - \frac{R}{2}\frac{t_o}{d(t_o - d)}}} \qquad (1)$$

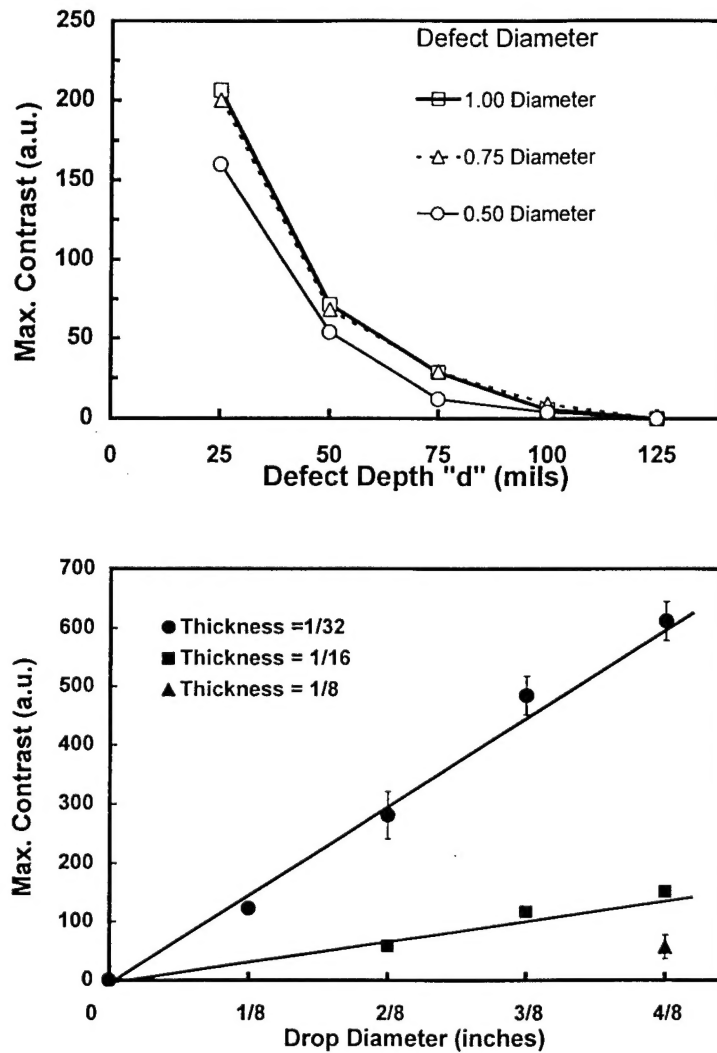Where the parameters are shown in Figure 5 (left) and represent:

Figure 4. (Top) This graph shows the contrast temperature for all flat bottom holes shown in figure 3a. (Bottom) This graph shows the contrast temperature for all panels with simulated entrapped water shown in Figure 3b.

ΔT_{cont} contrast temperature
Q   energy deposited on the surface of the sample per unit area
ρc is the specific heat times the density of the sample
d   distance from surface of the sample to the defect
t_o is the thickness of the sample
R   is the radius of the defect

This equation correctly accounts for all of the observed experimental results. The term before the square bracket provides the principal contribution to the thermal contrast from which the following can be verified:

1. The contrast temperatures (ΔT) increases linearly with the amount of energy deposited per unit area (Q).
2. The higher the specific heat-density of a material ($\rho c \uparrow$) the smaller the contrast temperature becomes ($\Delta T \downarrow$).
3. The closer the defect is to the surface (d → 0) the larger the contrast temperature becomes (ΔT → ∞).
4. As the defect depth approaches the panel thickness (d → t_o) the contrast temperature vanishes (ΔT → 0).
5. For a given defect depth d, the thicker the panel (t_o → ∞) the larger the contrast temperature ($\Delta T \uparrow$).

The term in square brackets represent the lateral heat flaw effects and the following can be verified:

6. As defects approach the surface (d → 0) or as they approach the far end (d → t_o), the lateral heat effects diminish ([lateral factor]→ 1) and the contrast temperature approaches $\Delta T = \dfrac{Q}{\rho c}\left(\dfrac{1}{d} - \dfrac{1}{t_o}\right)$.

7. When the defect size decreases (R → 0), the lateral heat factor vanishes ([lateral factor] → 0) and the thermal contrast disappears (ΔT → 0).

8. When the defect size increases (R → ∞), then lateral isolation is approached and the lateral heat effects diminish ([lateral factor] → 1) and the thermal contrast becomes $\Delta T = \dfrac{Q}{\rho c}\left(\dfrac{1}{d} - \dfrac{1}{t_o}\right)$

9. When the thickness of the panel becomes very large (t_o → ∞), the contrast temperature has the limiting value given by $\Delta T = \dfrac{Q}{\rho c}\dfrac{1}{d}\left(\dfrac{R}{2d}\right)^{1-\frac{R}{2d}}$

Similar analysis can be conducted for the problem of water entrapment. From the graph on Figure 4 (Top) it is clear that the thicker the panels are, the smaller the contrast temperature will be. Also, as the diameter of the defect gets smaller the contrast temperature diminishes. The error bars on the graph represent the effect that different amounts of water had on the thermal contrast. It is obvious from the smallness of the error bars that the effect of the amount of entrapped water on the thermal contrast is minimal. A simple model was previously obtained[3] that used a simple lateral heat approximation. The main result of the model is that the contrast temperature of a sample with water entrapped can be approximated by the following equation if a contact conductivity is used instead of the thermal conductivity, then

$$\Delta T_{peak} = \frac{Q}{\rho c}\frac{d}{r \cdot t_o^2}\cdot\left[\frac{h}{2k}\frac{R}{d}r\right]^{1+\frac{h}{2k}\frac{R}{d}r} \tag{2}$$

Where the parameters are shown in Figure 5 (right) and represent:

h   contact conductivity between aluminum and water
k   contact thermal conductivity of aluminum
r   specific heat-density ratio ($r = \rho c / \rho_w c_w$)
d   the height of the water drop
t_o is the thickness of the aluminum sample
R   is the radius of the water drop

This equation correctly accounts for most of the observed experimental behavior of pulsed thermography as it relates to water entrapment. The terms before the square bracket provide the principal contribution to the thermal contrast from which the following can be verified:
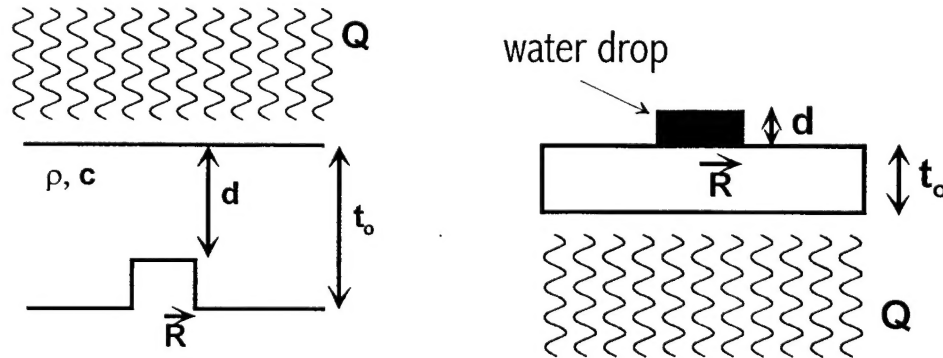

Figure 5. This illustration shows the main parameters used when modeling the thermographic process for mass loss due to corrosion (left) and water entrapment (right)

1. The contrast (ΔT) increases linearly with the amount of energy deposited (Q).
2. The higher the specific heat-density of the substrate ($\rho c \uparrow$) the smaller the peak contrast ($\Delta T \downarrow$).
3. The contrast temperature (ΔT) is a linear function of the radius R for small values of the term in brackets.
4. As the amount of water grows indefinitely ($d \rightarrow \infty$) the contrast temperature saturates ($\Delta T \rightarrow Q/\rho_1 c_1 t_o^2$).

CHARACTERIZATION OF CORROSION

There are various types of corrosion present in metallic structures such as pitting, exfoliation, filiform, galvanic and crevice corrosion. Since the first means of corrosion protection is by painting the exposed surface or by sealing joined parts, corrosion will always start as hidden. Some of the locations where corrosion can be found are under the paint, around fasteners, inside lap joints, behind panels and on second layers. The ability to detect corrosion thermographically will depend on the amount of contrast generated relative to other contrast generating non-uniformities. Figure 6 shows a thermal image of an aluminum lapjoint with three rows of fasteners. The fasteners appear dark because they are much thicker than the structure being interrogated. Around several of the fasteners there are regions that clearly appear brighter than others as indicated in the figure. These regions can be interpreted as probable corrosion regions, but due to the proximity of the fasteners and the fact that sealant was used, it is difficult to determine if any mass has been lost. At the time of this paper the part could not be cut open in order to make a definite assessment of the defect. In order to make an exact determination of the cause for the hot regions a better knowledge of the part and finite element calculations are needed.

DETECTABILITY REGION

There is a "rule of thumb" that is regularly used to determine the ultimate depth to which a defect of a given size can be detected by thermal methods. This rule states that "those planar defects located at a depth smaller or equal to their cross sectional diameter can be detected thermographically". In light of the simple models presented in this paper, this rule of thumb is not precise. From eq. 1 it can be seen that any planar defect, no matter what its location or cross section, can be detected thermographically provided that enough energy is deposited on the sample surfaces. This is direct consequence of the linear dependence of the thermal contrast on the amount of energy deposited on the surface. There is of course a practical limit of not depositing so much energy so as to damage the material.

More insight can be obtained into this matter by inverting eq. 1 and obtaining a relation between the size of the flaw "2R" and the distance of the flaw from the surface of the sample "d". The following equation is obtained

$$R = 2\frac{d(t_o - d)}{t_o} \cdot finv\left[\frac{\Delta T_{contrast}\rho c}{Q \cdot \left(\frac{1}{d} - \frac{1}{t_o}\right)}\right] \tag{3}$$

where the function "finv[x]" is the inverse of the transcendental function $y=x^{1/(1-x)}$. This equation can be used to divide the R-d space into "detectable" and "non-detectable" regions. That is, a defect whose radius "R" and location "d" are such that it
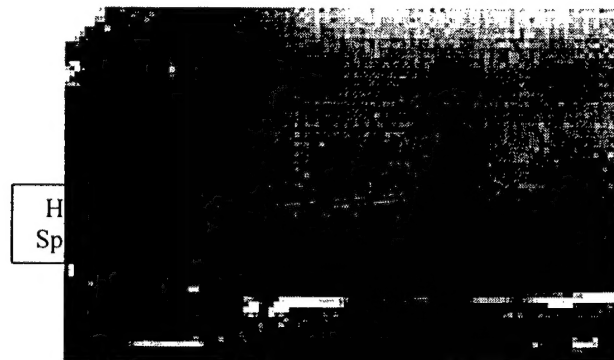

Figure 6. Aluminum lapjoint with three rows of fasteners. There is clear evidence of a hot spots around some fasteners.
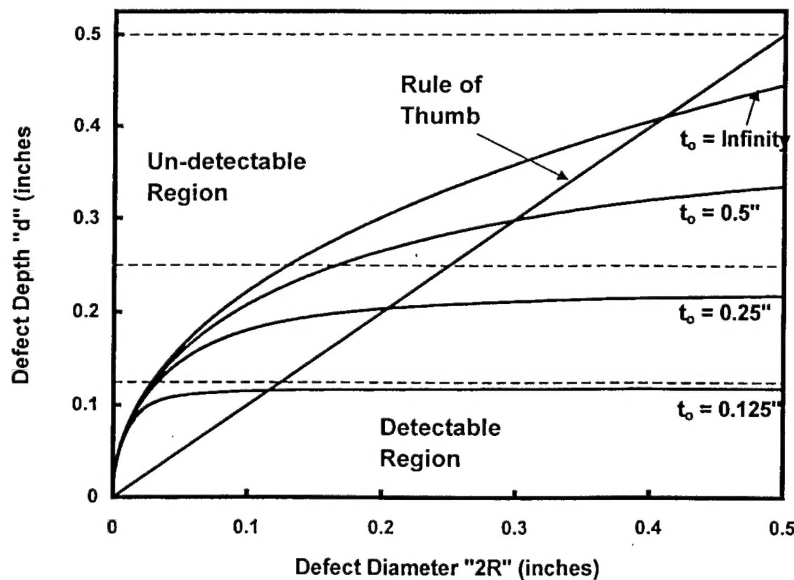
Figure 7. This graph shows curves that separate detectable from undetectable regions of defect of diameter 2R.

falls inside the curve defined by equation 3 will be detectable thermographically. If the defect radius and position are such that they fall outside the curve, then for those experimental parameters the defect will be missed. Figure 7 shows boundary curves for various aluminum thickness. Also on that graph is the "rule of thumb" line. Clearly there is a strong discrepancy between the rule of thumb and the previous results.

SUMMARY

We have demonstrated that thermography can detect mass loss and water entrapment. We have presented predictive formulas that can assist the practitioner in determining what type of contrast levels will be obtained for a particular experimental arrangement. We have determined what the depth of resolution is for the detection of mass loss in aluminum 7075T6. When interrogating real structural components, these simple models can only provide approximate answers. For precise determination of the exact nature and extent of the defect a detailed knowledge of the part is required together with more detailed analysis such as finite element models.

ACKNOWLEDGMENT

REFERENCES

1   I. Perez, R. Santos, P. Kulowitch, M. Ryan, "Calorimetric modeling of thermographic data," Proc. of the 1998 SPIE Thermosense XX Conference", Orlando, April 6 - 9, 1998

2   I. Perez, P. Kulowitch, "Modeling of Pulsed Thermography in Anisotropic Media," 25th annual Progress in QNDE, Snowbird, Utah., July 19 - 24, 1998

3   I. Perez, W. R. Davis, P. Kulowitch, "Thermographic modeling of water entrapment," Proc. of the 1999 SPIE, Thermosense XXI Conference, eds. D.H. LeMieux & J.R. Snell, Jr. April 1999, p32-39
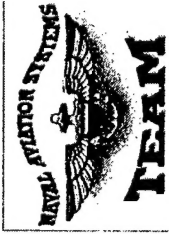
THERMOGRAPHY FOR CHARACTERIZATION OF CORROISON DAMAGE

Ignacio Perez, Paul Kulowitch

Naval Air Warfare Center

Aircraft Division, Patuxent River, MD

CORROSION/2000
NACE's Annual Conference

Orange County Convention Center

Orlando,Florida
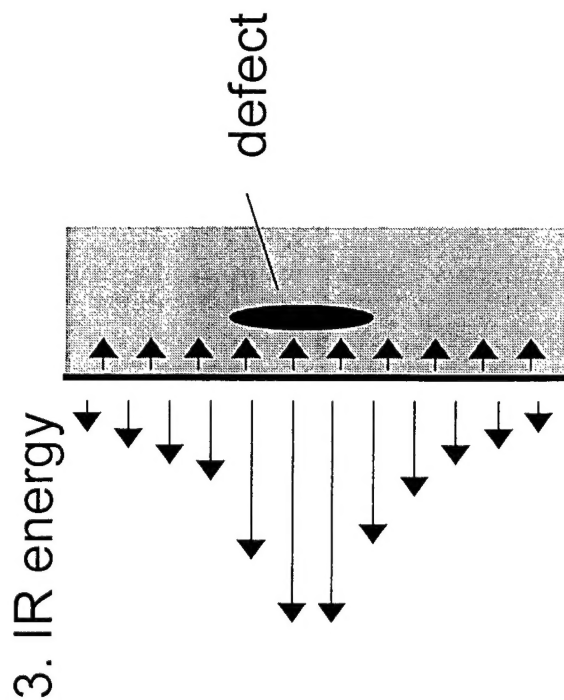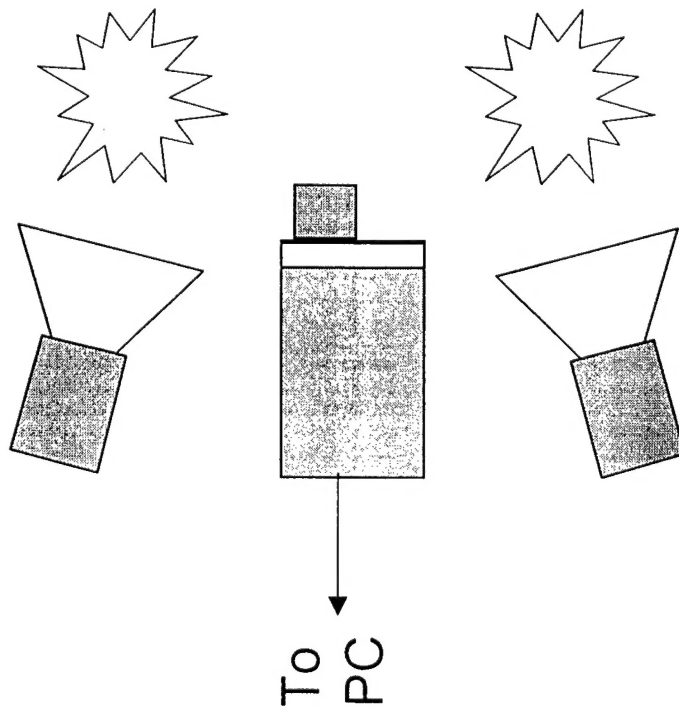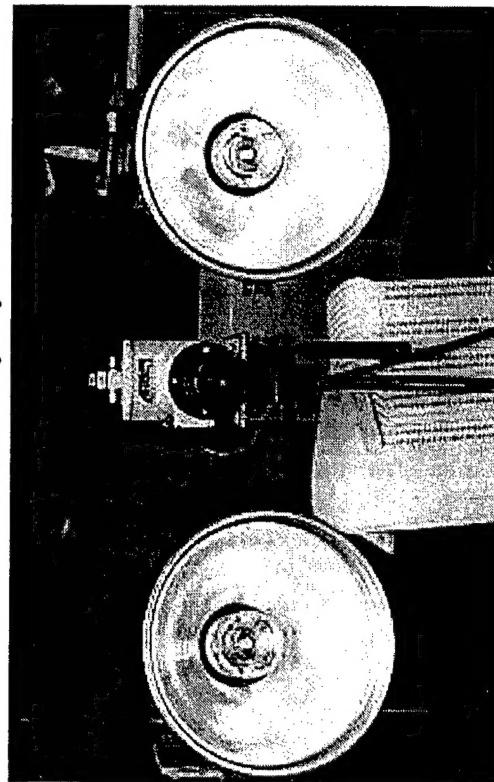
March 26 - 31, 2000

Outline

- Experimental

- Data analysis

- Simple calorimetric model

- Simple few element model

- Experimental results
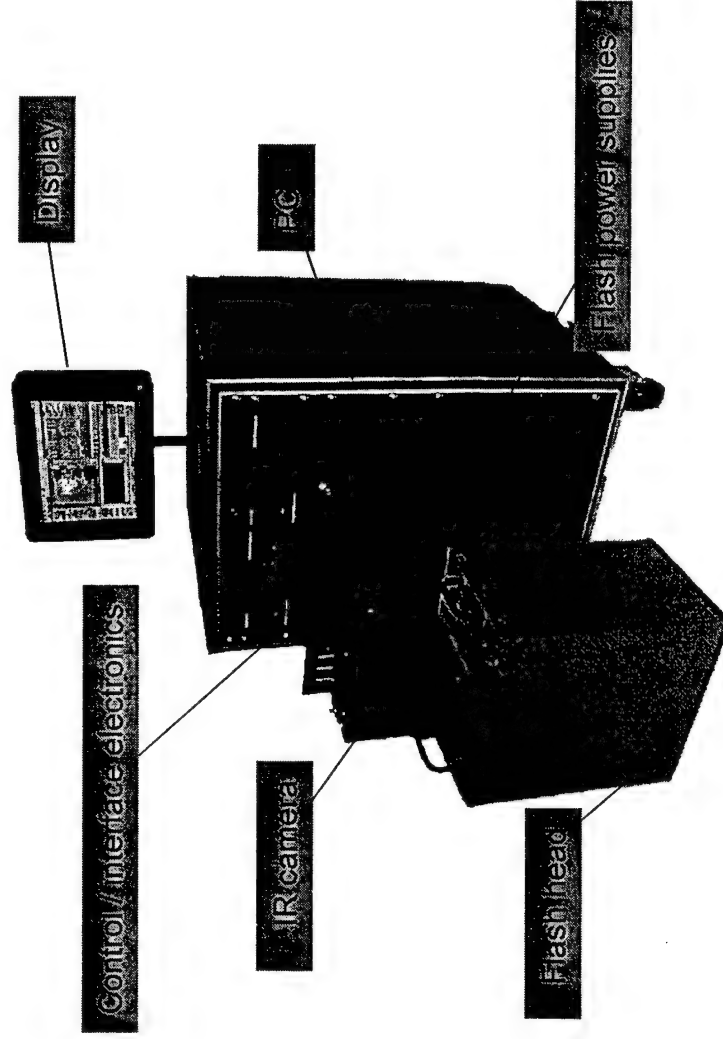
- Expanded model

- Summary and conclusion

Basics

3. IR energy

defect

1. Light

To
PC

Laboratory System

The EchoTherm® System

- Camera independent
- Portable imaging head
- Uniform flash heating
- Integrated acquisition, excitation, and analysis
- Scriptable and programmable
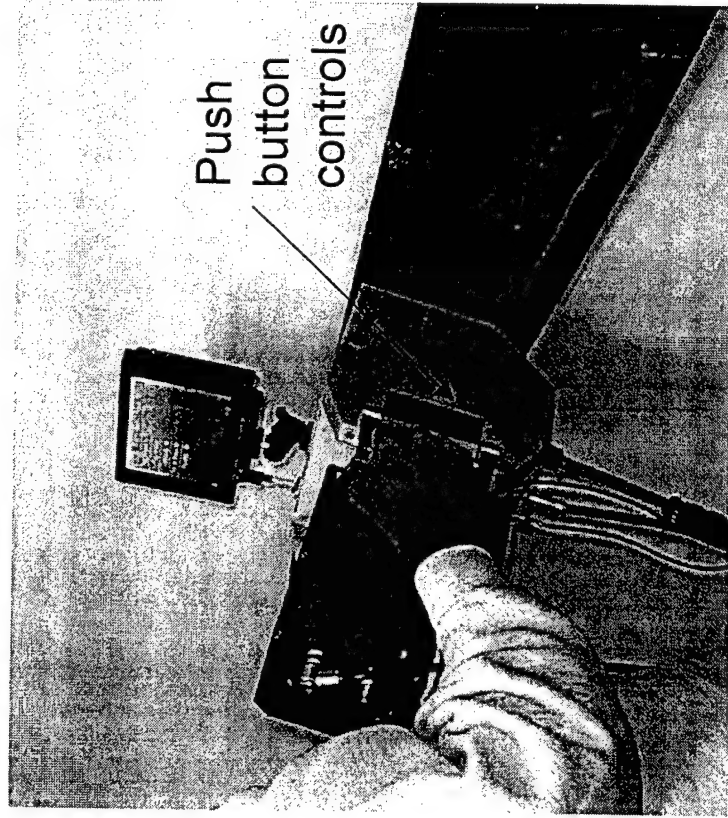- Auto analysis capability
- Single operator
- Remote operation and display

Diagram labels: Display, PC, Flash power supplies, Control / interface electronics, IR camera, Flash head

NAVAL AVIATION SYSTEMS TEAM

Next Generation System

Inspection Head
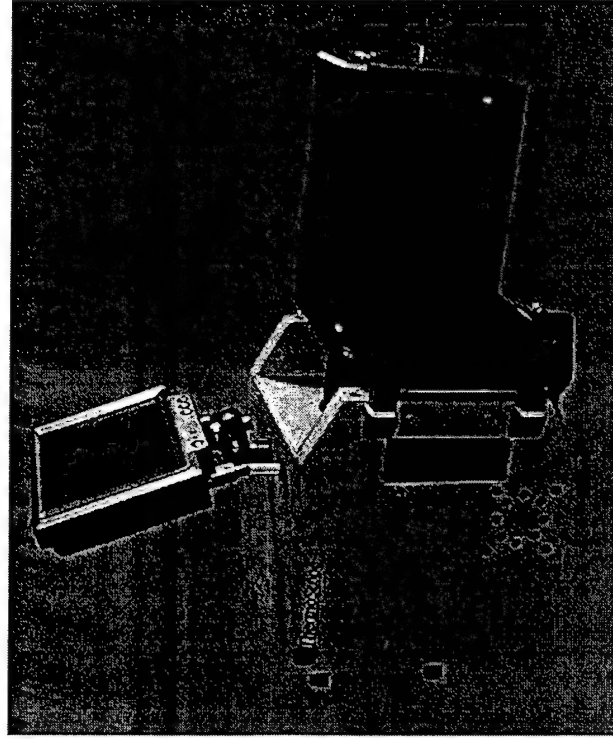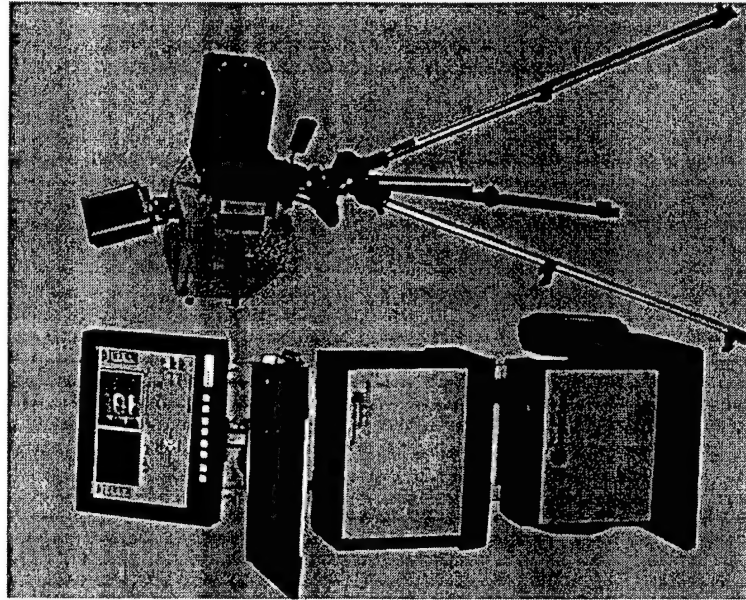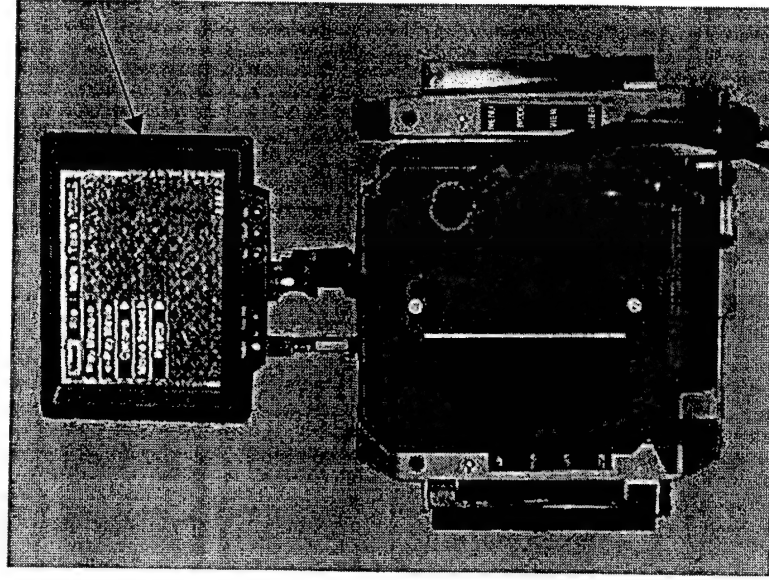
Display calculated results

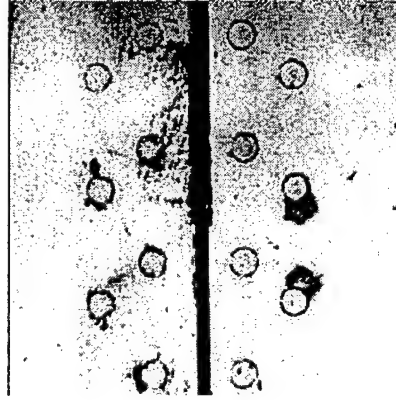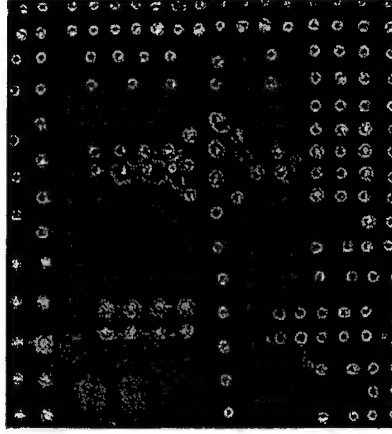Push button controls

ThermoScope™

Data
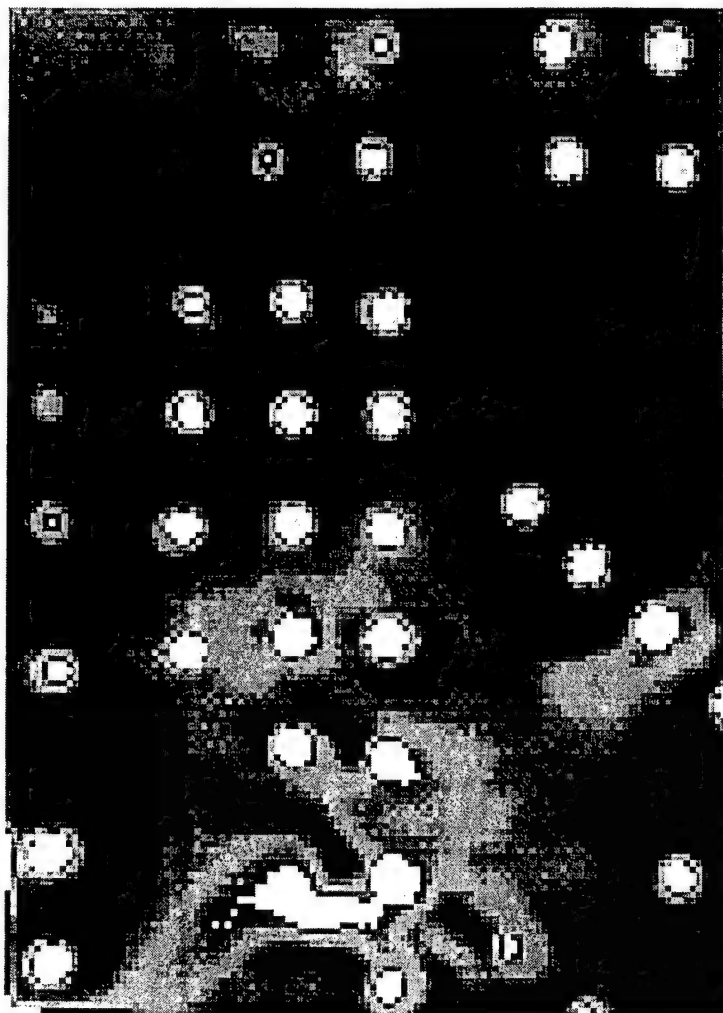
Advantages

Thermography has a demonstrated capability for detection of distributed subsurface defects (e.g. corrosion, voids, delamination). It offers the advantages of speed, noncontact detection, and wide-area coverage.
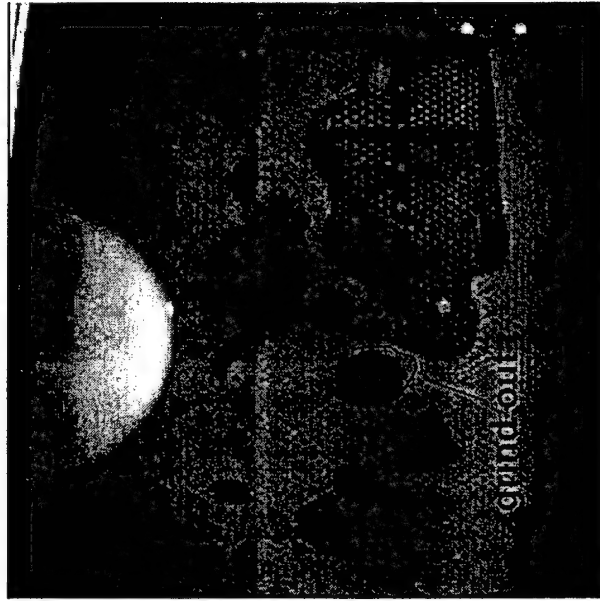
Backsurface Corrosion

Near Surface Corrosion (exfoliation)

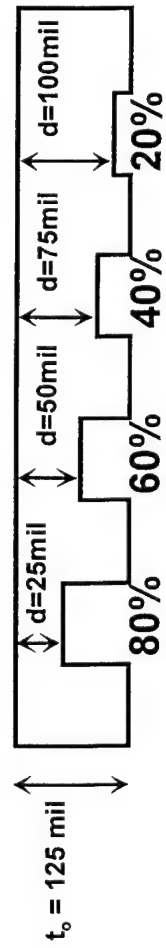# Uniform Flash Thermograghy Result: F-18 Splitter Plate Corrosion

Flash Thermographic Image

White areas indicate corrosion that was not previously detected.

Preflash Image

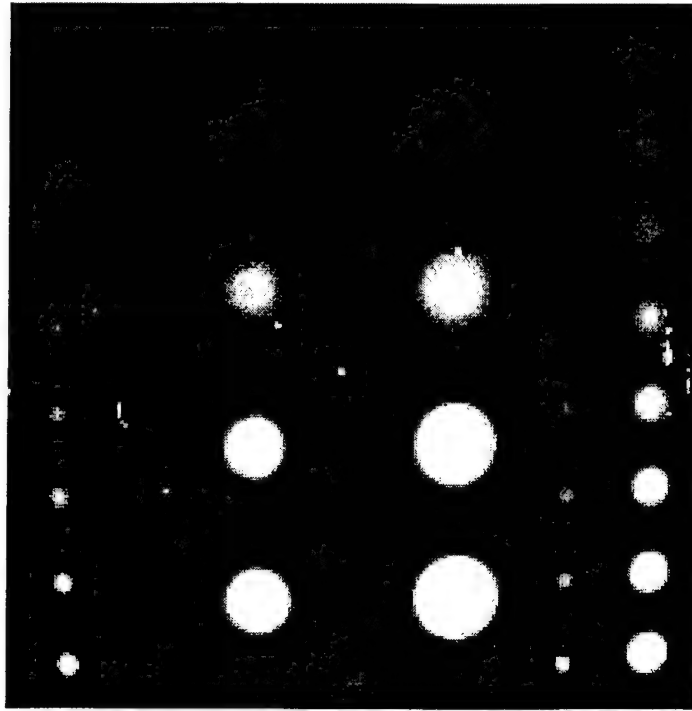In darker gray areas corrosion indications have been ground out.
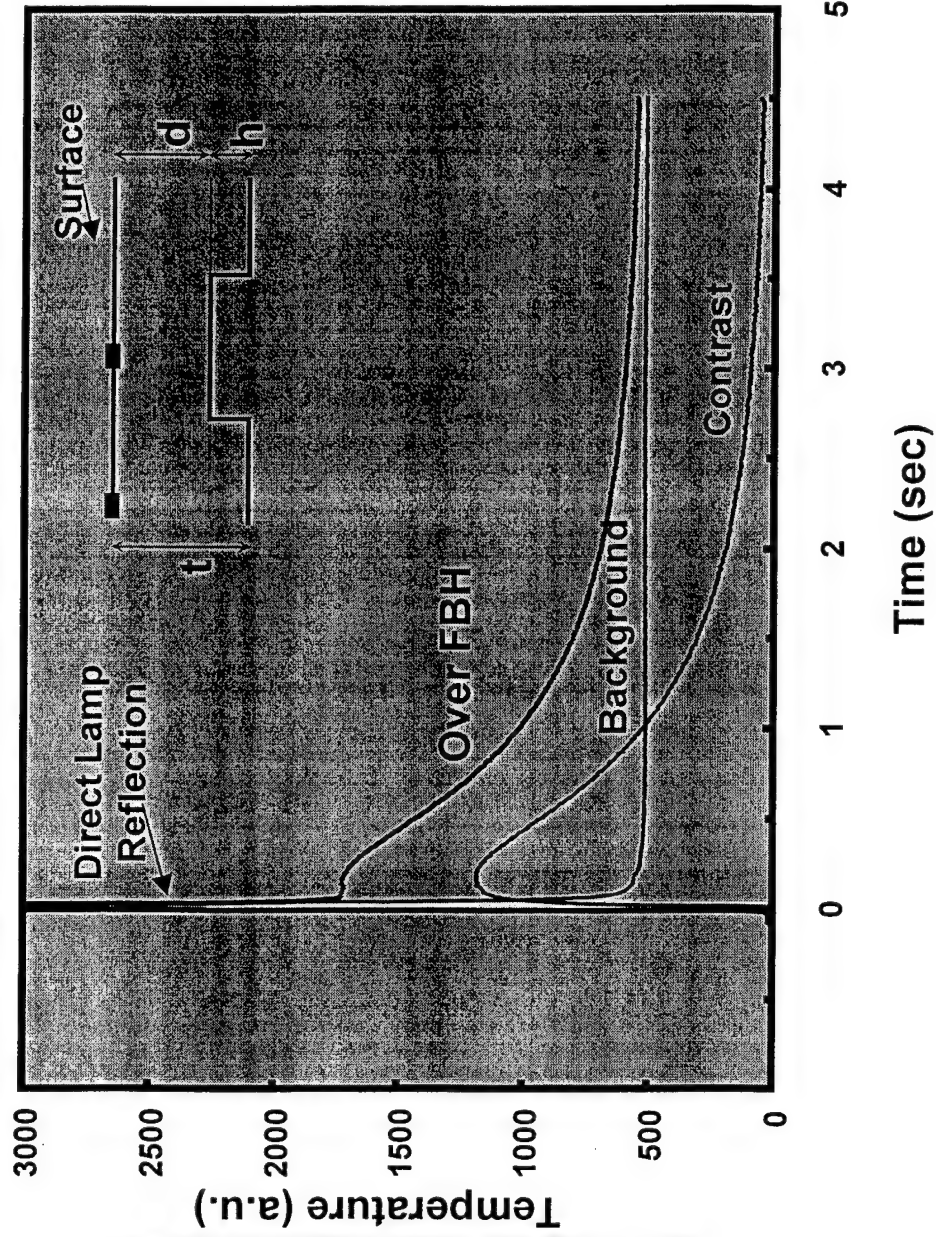
Flat Bottom Hole Standards

$t_0 = 1/8''$
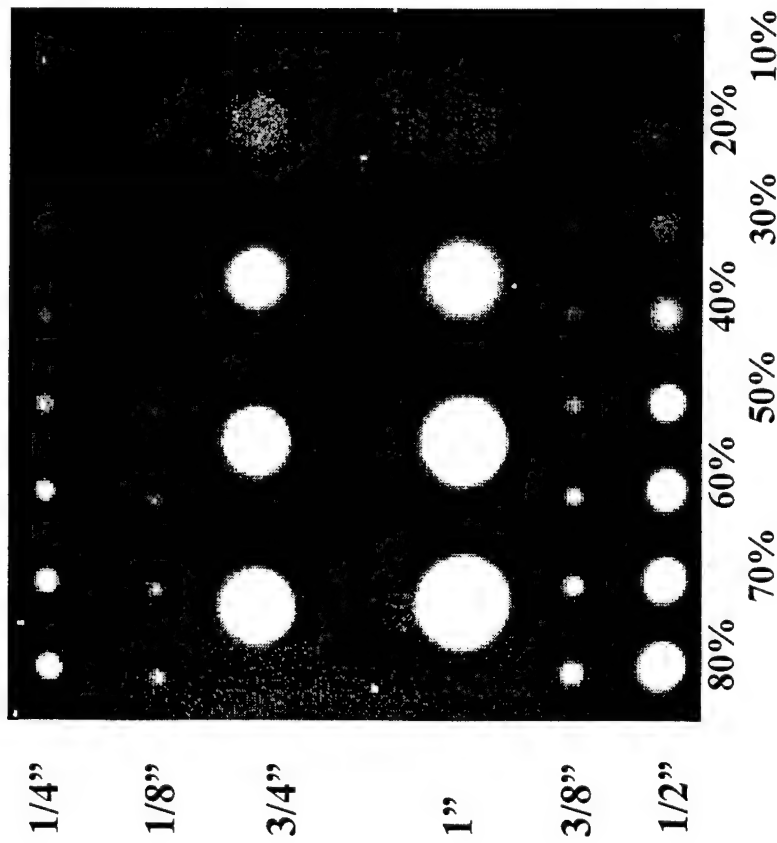
$t_0 = 3/8''$
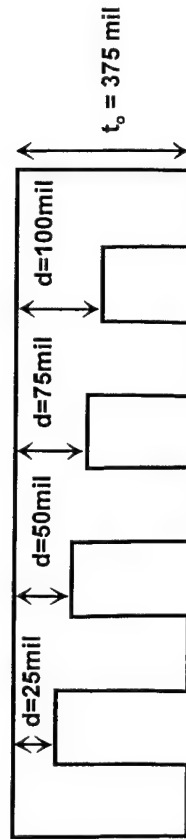
Contrast Curve Generation

$t_o = 1/8''$
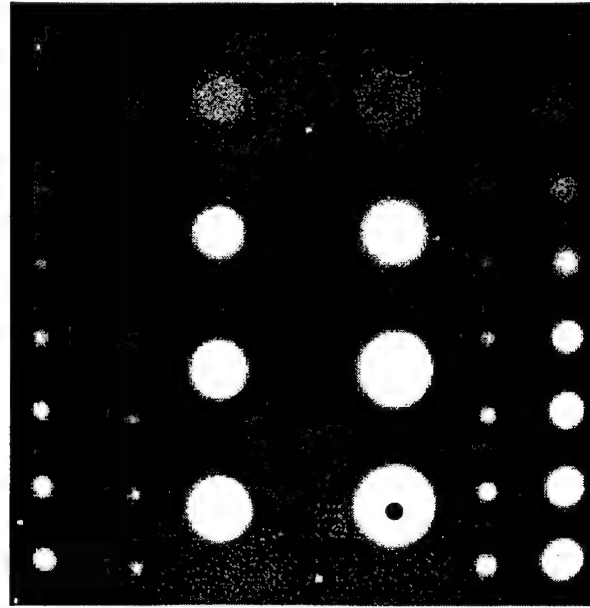
Contrast Curves
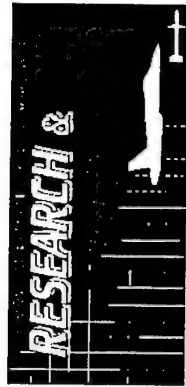
Diameter 1"

$t_0 = 1/8"$
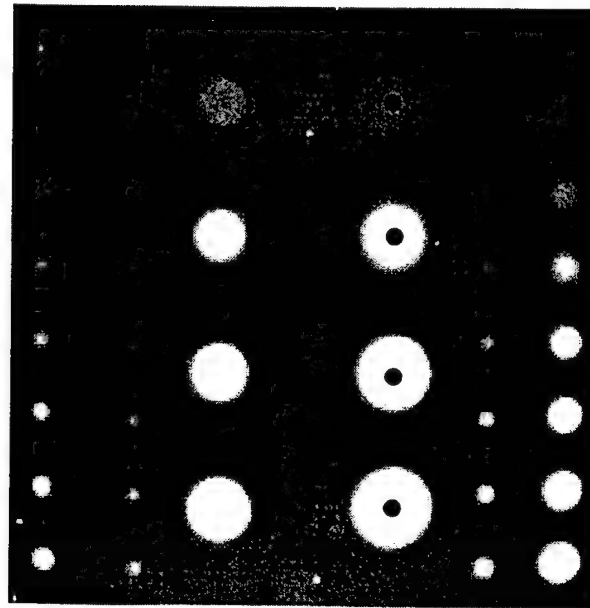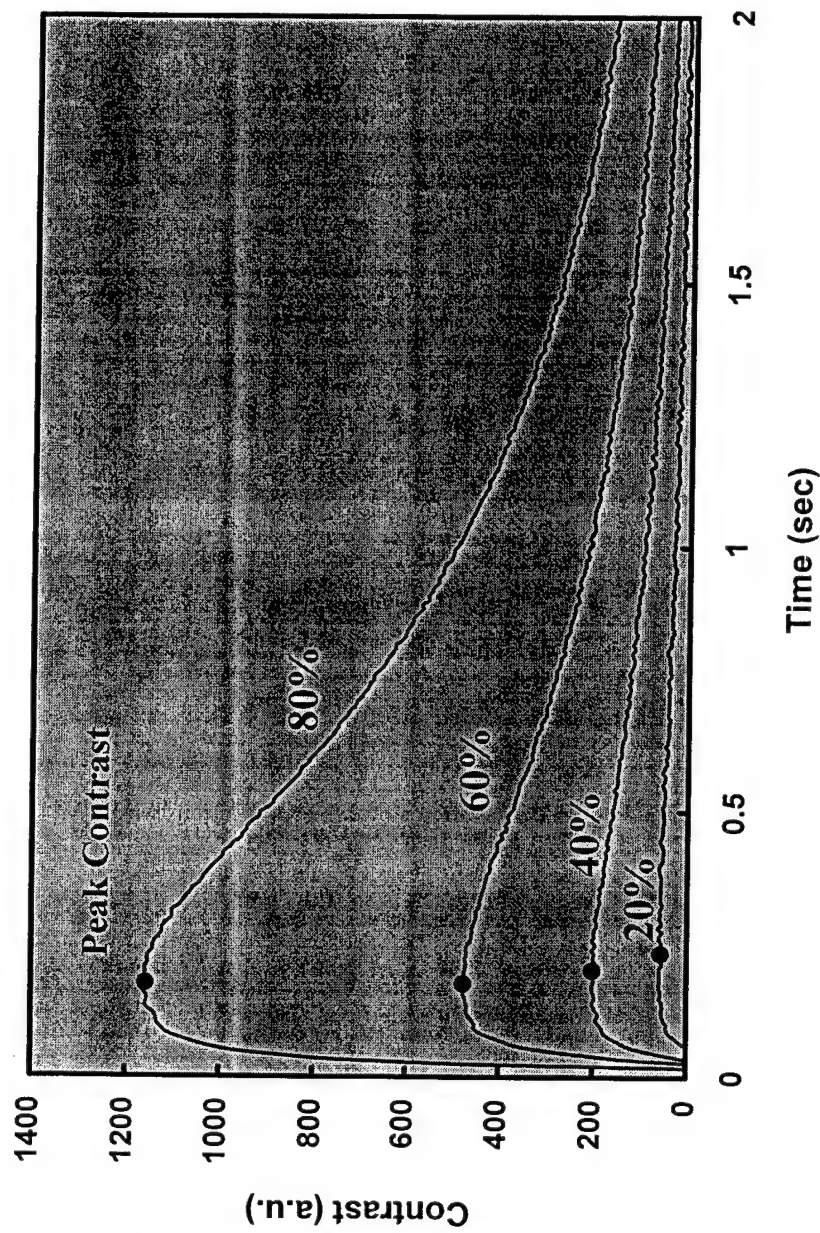
Peak Contrast vs Defect Depth
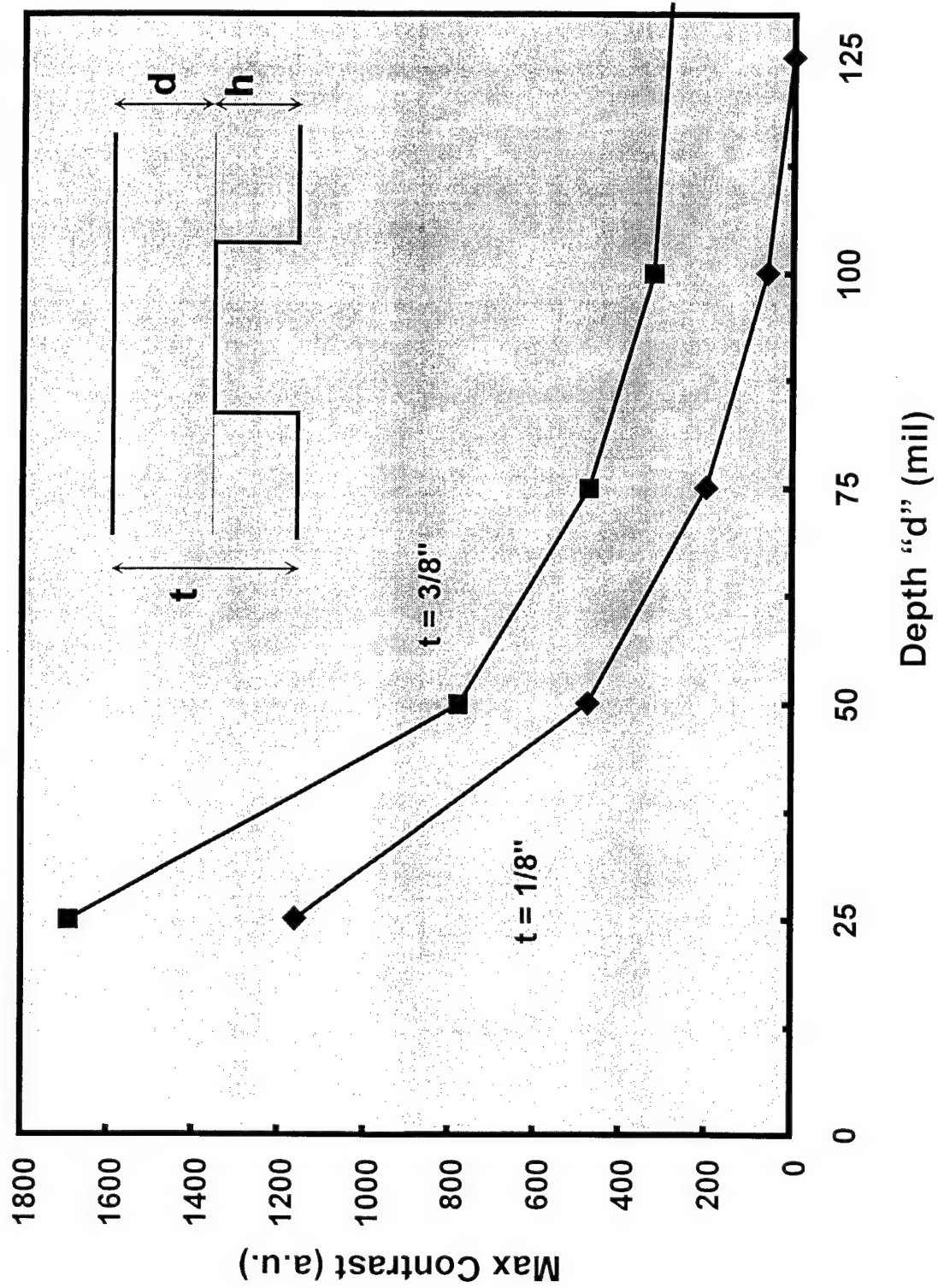
Simple Model
(no lateral heat effects)

NO LATERAL CONDUCTION APPROXIMATION

$$q = m \cdot c \cdot \Delta T$$
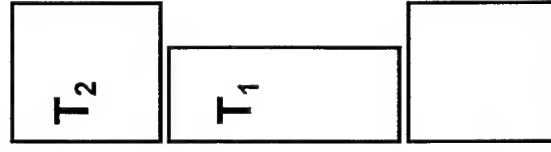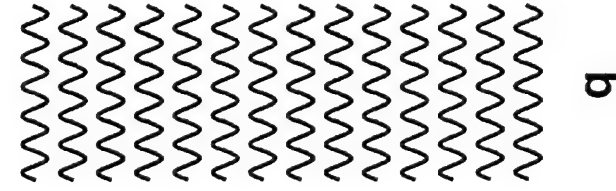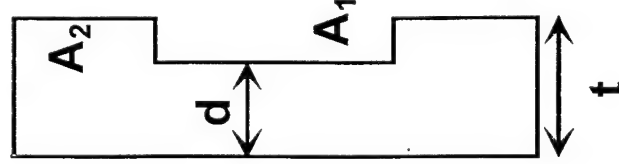
$$q_2 = \rho \cdot A_2 \cdot t \cdot c \cdot T_2$$

$$q_1 = \rho \cdot A_1 \cdot d \cdot c \cdot T_1$$

$$\Delta T = \frac{Q}{\rho \cdot c} \left(\frac{1}{d} - \frac{1}{t} \right)$$

$\Delta T = T_1 - T_2$

$Q = q/A$

FLAT BOTTOM HOLE
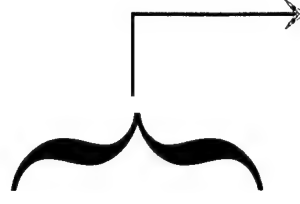
Contrast Properties

$$\Delta T = \frac{Q}{\rho \cdot c}\left(\frac{1}{d} - \frac{1}{t}\right)$$

- The contrast (ΔT) increases linearly with the amount of deposited energy per unit area (Q).

- The higher the specific heat-density of a material ($\rho c\uparrow$) the smaller the peak contrast ($\Delta T\downarrow$)

- The closer the defect to the surface (d $\rightarrow$ 0) the higher the peak contrast ($\Delta T \rightarrow \infty$).

- As the defect depth approaches the panel thickness (d $\rightarrow$ t) the contrast vanishes ($\Delta T \rightarrow 0$).

- For a given defect depth d, the thicker the panel (t $\rightarrow \infty$) the larger the contrast ($\Delta T \rightarrow q/\rho cd$).

Effects of Energy Deposited on Surfa...

DEPTH OF RESOLUTION vs ENERGY
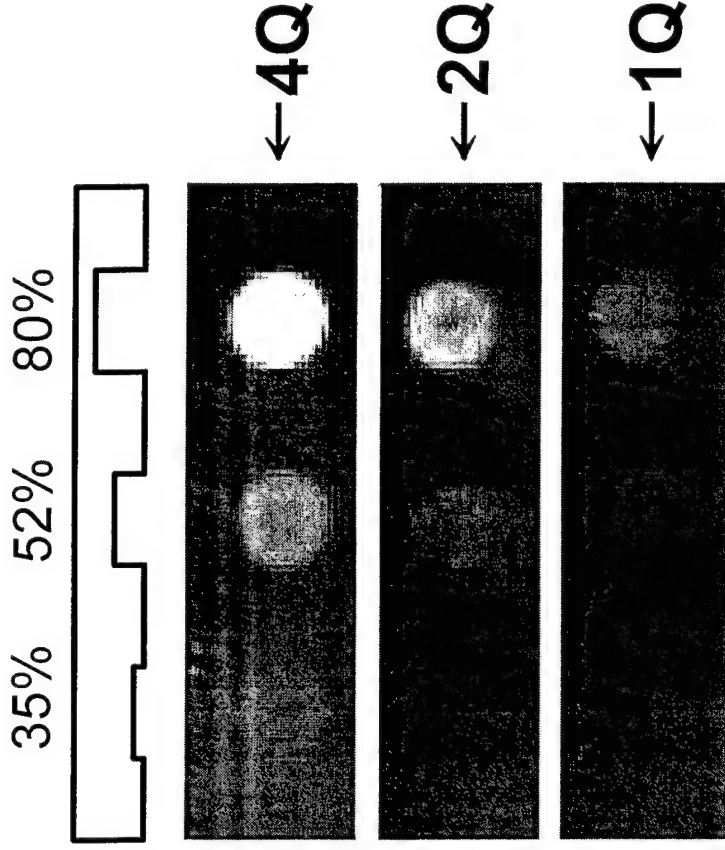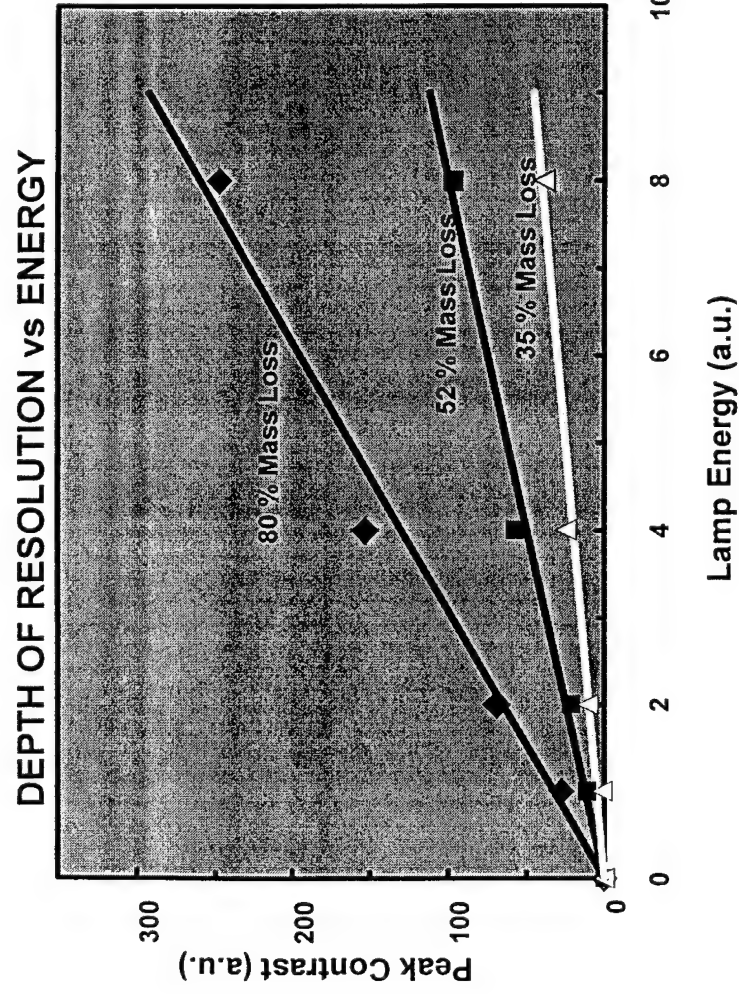
- The contrasts temperature decreases linearly as the amount of energy deposited on the surface decreases

Fit to Experimental Data

Peak Contrast
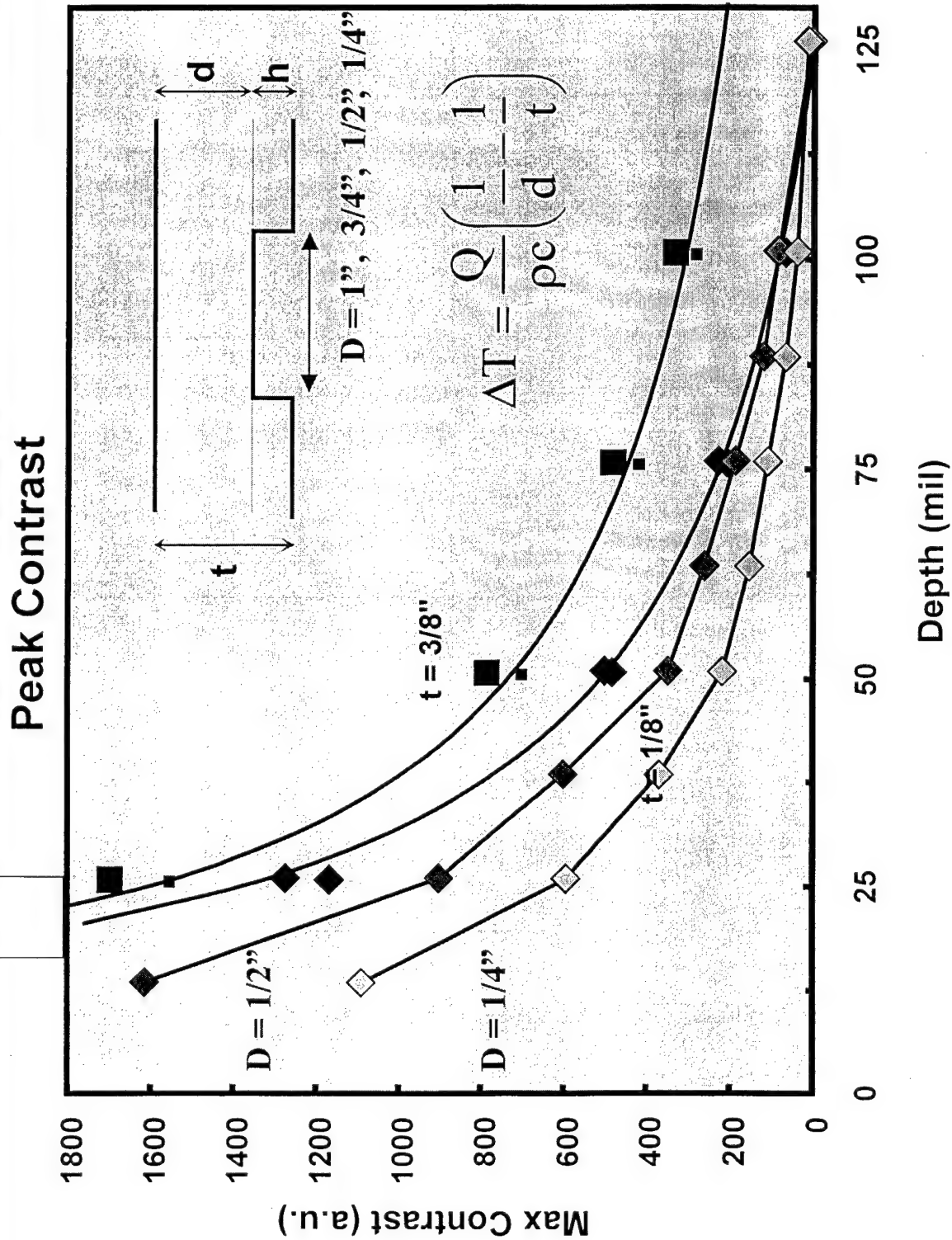
Lateral Heat Flow Model
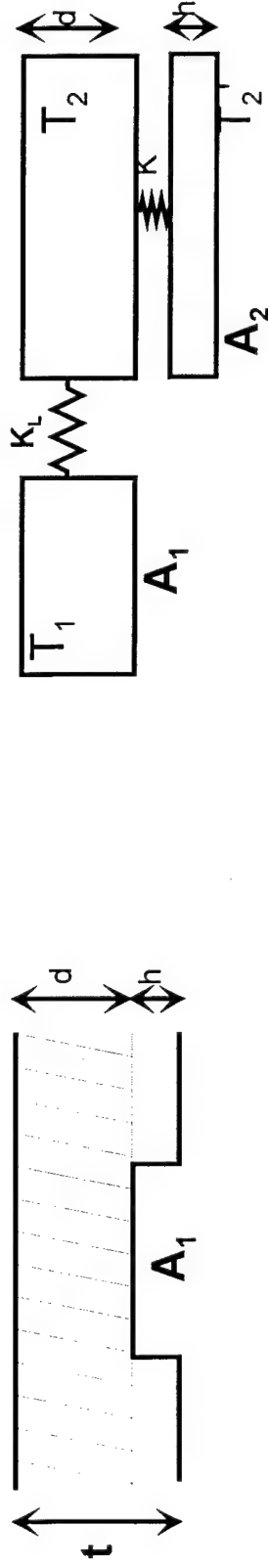
$$\rho \cdot A_1 \cdot d \cdot c \cdot \frac{dT_1}{dt} = K_L \cdot (T_2 - T_1)$$

Apply energy conservation to each element, then

$$\rho \cdot A_2 \cdot d \cdot c \cdot \frac{dT_2}{dt} = K_L \cdot (T_1 - T_2) + K \cdot (T_2' - T_2)$$

$$\rho \cdot A_2 \cdot h \cdot c \cdot \frac{dT_2'}{dt} = K \cdot (T_2 - T_2')$$

$$f_L = x^{\frac{1}{1-x}}$$

$$\Delta T = \frac{Q}{\rho c}\left(\frac{1}{d} - \frac{1}{t}\right) \cdot f_L$$

$$x = \frac{1}{2}\frac{K}{K_L}\frac{R \cdot t}{d \cdot h}$$

Lateral Factor

Lateral Heat Factor

Chart: Lateral Factor $f_{lateral}(d)$ (y-axis, 0 to 1) vs Depth "d" (inches) (x-axis, 0 to 0.125)

Legend:
- R = 2.00 inches
- R = 1.00 inches
- R = 0.50 inches
- R = 0.25 inches
- R = 0.13 inches
- R = 0.06 inches

Curve labels: R = 2", R = 0.5", R = 0.06"
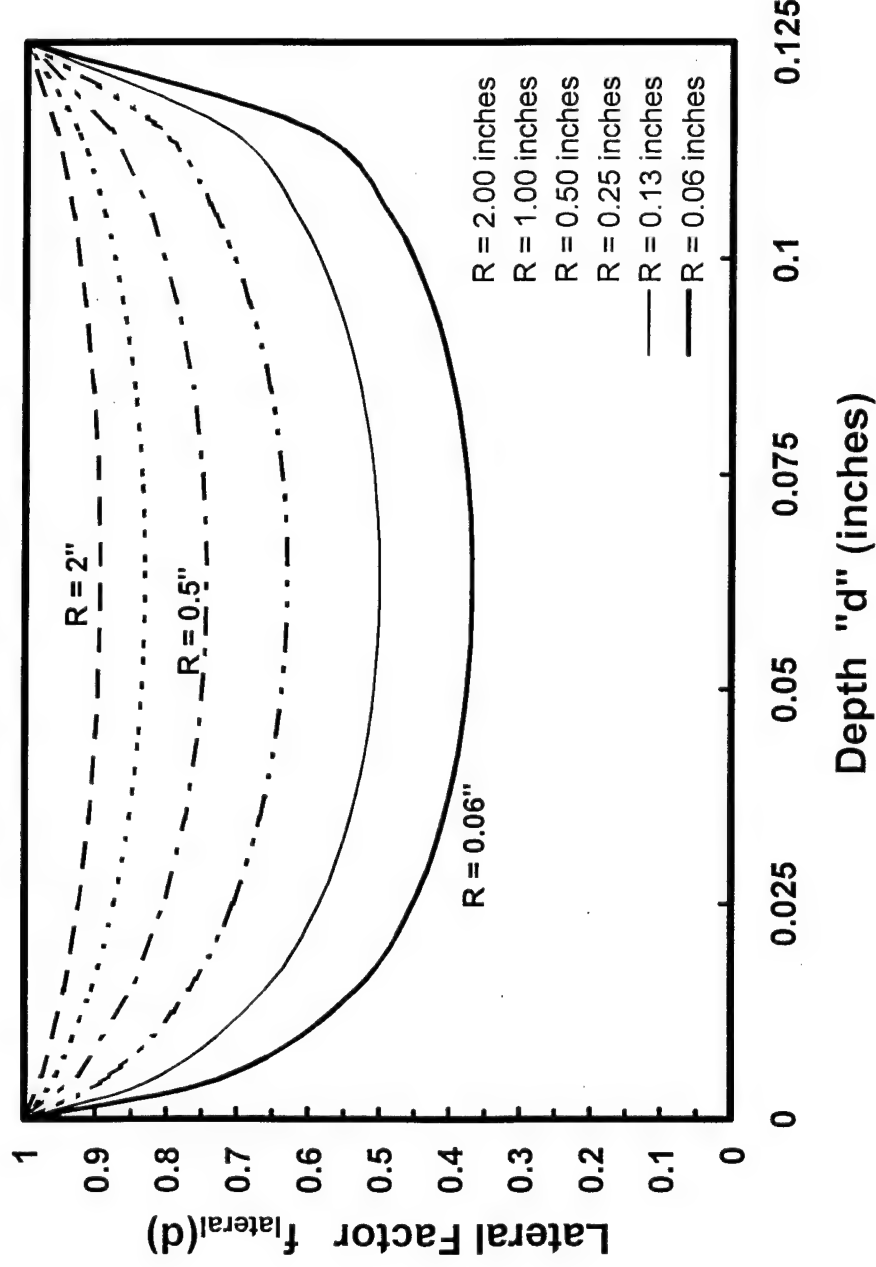
$$\Delta T = \frac{Q}{\rho c} \left(\frac{1}{d} - \frac{1}{t} \right) \cdot f_L$$

where

$$f_L = x^{\frac{1}{1-x}} = \left(\frac{1}{2} \frac{K}{K_L} \frac{R \cdot t}{d \cdot h} \right)^{\frac{1}{1 - \frac{1}{2} \frac{K}{K_L} \frac{R \cdot t}{d \cdot h}}}$$

Detectable Region
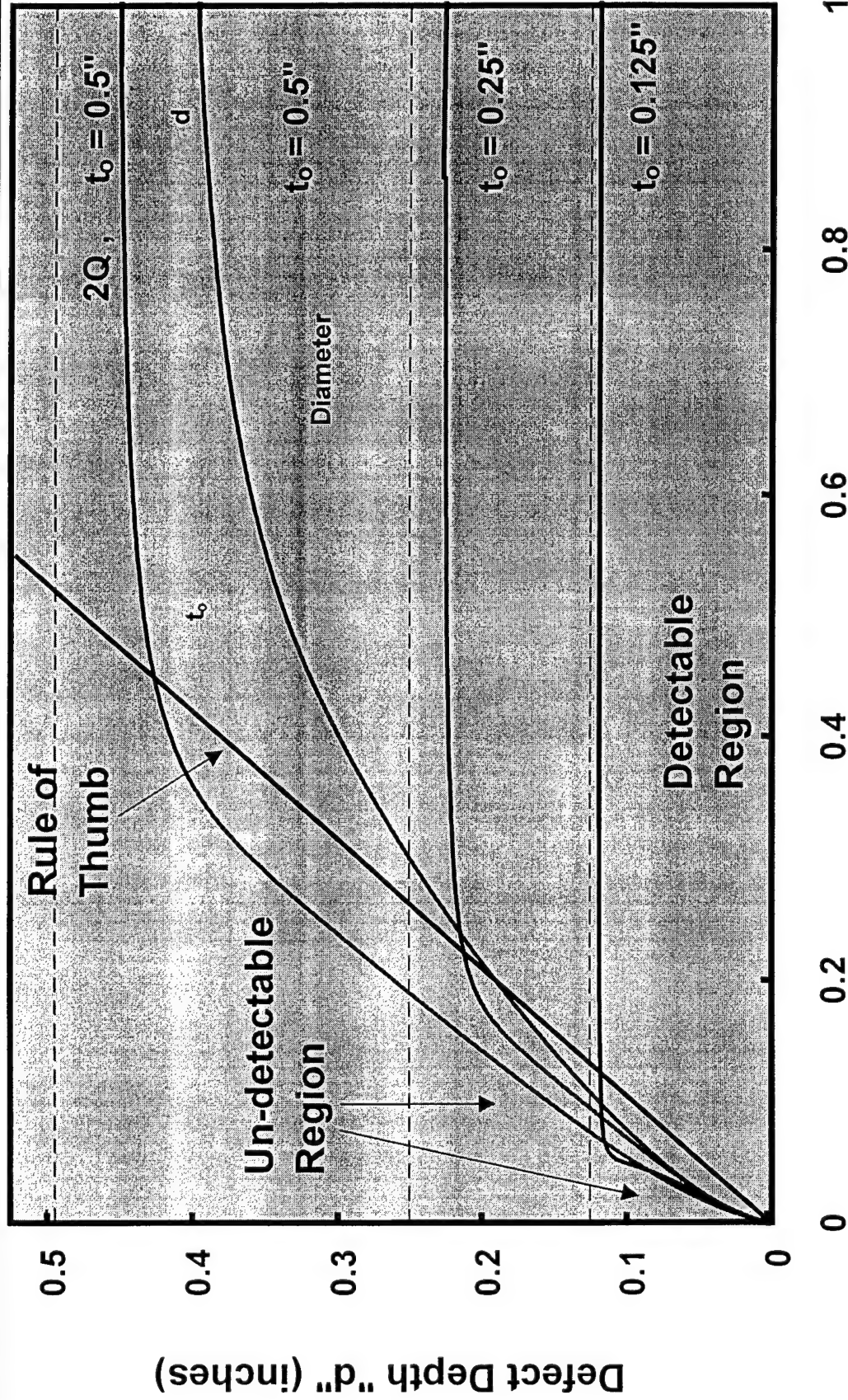
Defect Diameter "2R" (inches)

Thermographic modeling of water entrapment

Ignacio Perez, William R. Davis, Paul Kulowitch
Naval Air Warfare Center, Materials Division
Patuxent River MD, 20670

M. Frederick Dersch
Naval Surface Warfare Center
Survivability, Structures and Materials Directorate
Carderock, MD 20817

ABSTRACT

A common problem found in advanced structural materials is water entrapment. This problem is a major cause of material degradation. In metals it can lead to corrosion and in composites it adds unnecessary weight to the structure and can lead to material degradation especially after freezing and thawing. Thermography has been investigated as a means of detecting water entrapment in metallic structures. A simple model has been derived that accurately describes the thermal response of these structures to short heat pulses. In this paper results on Aluminum panels with various amounts of water entrapment will be presented. Sensitivity relations will be derived and validated.

Keywords: NDE, thermography, thermal models, calorimetric models, defects, water entrapment

1. INTRODUCTION

The detection of entrapped water behind metallic structures is a difficult problem to solve in a nondestructive manner. X-ray radiography is commonly used [1] to detect the entrapped water but the technique is not very portable in general and requires special safety precautions. Ultrasonic attenuation methods have been successfully used but suffer from a lack of lateral resolution. In this paper experimental thermographic results and simple thermographic models will be presented and discussed.

Simple thermographic models have been previously introduced [2, 3] to successfully model the surface temperature evolution of panels with flat bottom holes. In those papers the hole diameter and depth were varied to simulate different amounts of mass loss due to corrosion. In all cases those simple thermographic models sufficed to accurately predict the maximum contrast temperatures observed in the experiments. This paper will closely follow the format and spirit of the previous references. Once again it will be seen that simple physical arguments go a long way in describing complicated thermal phenomena.

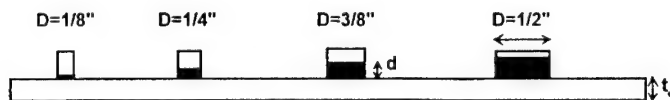Fig. 1: (Left) Drawing indicating key parameters used in study. Straws of various diameters (ranging from D = 1/8" to 1/2") were glued to aluminum panels of different thickness "t_0". The straws were filled with various amounts of water "d". (Right) Shows a single thermographic frame some time after a heat pulse. The dark regions in the image represent cold spots due to the presence of water in the back of the panel.
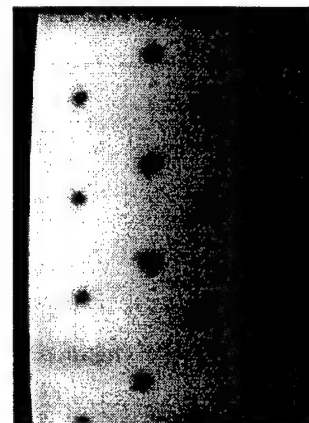
Experimental Parameters for Drops and Panels		
Al Thickness	Straw Diameter	Water Height
t_o = 1/32"	D = 1/8"	d = 0"
t_o = 1/16"	D = 1/4"	d = 1/16"
t_o = 1/8"	D = 3/8"	d = 1/8"
	D = 1/2"	d = 3/16"
		d = 1/4"

Table 1: This table shows the range of parameters used in this study

In this paper a simple theoretical model that contains all the relevant parameters required to describe the thermal transient process of aluminum panels with water entrapment will be presented. Some of the parameters used in the model include the amount of entrapped water, the diameter of the region with entrapped water, lateral heat flow effects, anisotropic properties, finite thickness effects of the metal plate and of the water column. In spite of the simplicity of the model, it will be seen that the model fits the experimental data remarkably well.

2. EXPERIMENTAL METHOD

The panels used in this study were imaged using a commercial pulsed IR NDT system (EchoTherm®, Thermal Wave Imaging, Inc.). Flash heating was provided by 2 linear xenon flashtubes with 5 msec flash duration, each powered by a 6.4 kJoule capacitor bank. The system was equipped with a 256 x 256 pixel InSb focal plane array camera (Radiance HS, Raytheon Amber) operating in the 2-5 micron spectral range. Continuous 12-bit data was acquired at a 120 Hz frame rate for 6 seconds after flash heating.

The material used in this study was aluminum 7075-T6. To model water entrapment, straws of different diameter were glued to the back of the panel and filled with water to various heights. Fig. 1 (Left) shows a drawing with some of the key parameters used in the model. The parameters "t_o", "D" and "d" represent the thickness of the panel, the diameter of the straws and the height of water added to the straws respectively. Three different thicknesses were chosen for the aluminum panels. Four different straw diameters were studied. The straws were filled with water to different heights. A total of 48 (3x4x4) different conditions were studied. Table 1 summarizes all the parameters used in fabricating these panels. The front side of the panels were painted with a flat black paint to avoid emissivity variation problems. The actual frame taken soon after the thermal flash was shot is shown in Fig. 1 (Right). The dark areas in that photo indicate the presence of water in the back side of the panel. The straws were staggered so as to keep the water as far as possible from one another minimizing
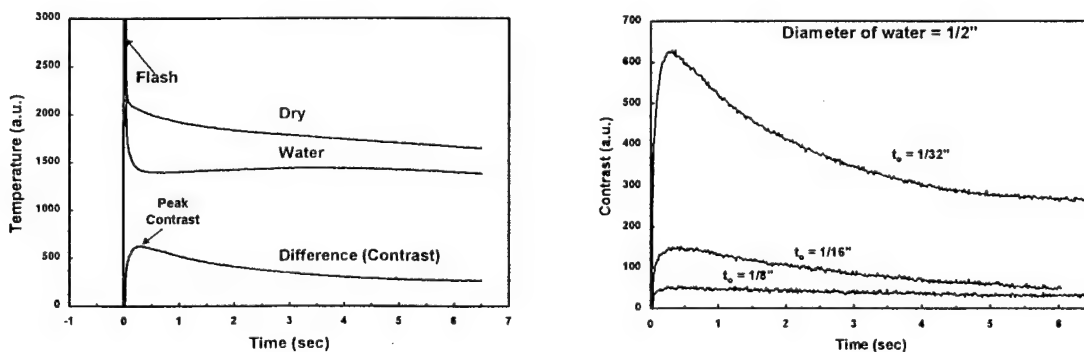
Fig. 2: (Left) This fig. shows the data curves require to generate a single contrast curve. The curve labeled "Water" represents the thermal time history of a point on the surface of the aluminum panel directly beneath a straw with filled with water. The curve labeled "Dry" represents the thermal time history of a point away from any water. The contrast curve was generated by subtracting the previous two curves. (Right) This figure shows three contrast curves for three identical water drops but for three different aluminum plate thickness.
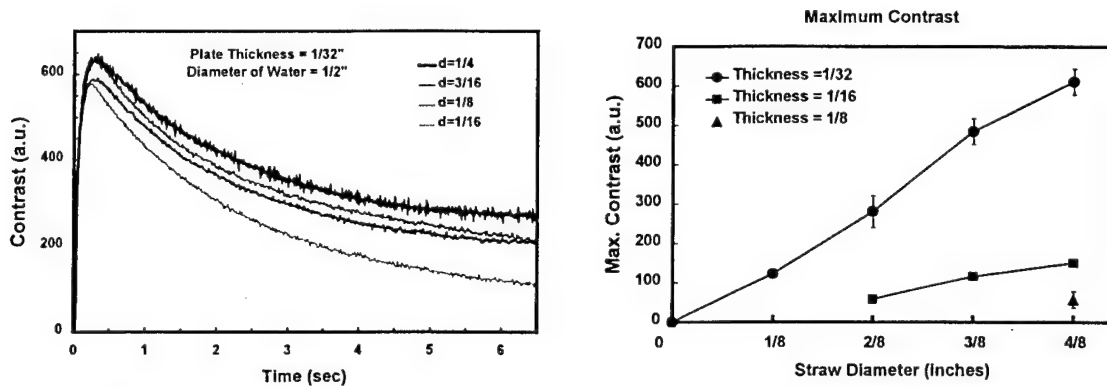
Fig. 3: (Left) This fig. shows four contrast curves for a given aluminum plate thickness and straw diameter but for four different water heights. (Right) This fig. shows the relation between the "maximum temperature contrast" for three aluminum plate thicknesses and four straw diameters.

interaction effects while maximizing the number straws in one panel.

3. EXPERIMENTAL RESULTS

In a standard experiment, digital data acquisition begins a few frames before the capacitor banks are discharged through the Xenon arc lamps. In our experiments the frame rate was set to 100 frames/sec. A total of 660 frames were acquired and the entire experiment lasted over 6.6 sec. Fig. 2 (Left) shows the entire thermal history of two points on the surface of the panel. The curve labeled "water" was taken from a point directly below and in the center of a straw containing some amount of water. This curve characterizes the thermal evolution a typical site that has some water over it. The curve labeled "dry" was taken from a point far away from any straw containing water and characterizes the thermal history of a dry aluminum block. Notice that the thermal history curve labeled "water" decays faster and to a lower value than the thermal history curve labeled "dry". This is due to the fact that the "water" acts like a thermal sink, thereby producing a decrease in the surface temperature. Also notice that the "water" curve and the "dry" curve have a region at early times with very elevated effective temperature. This region of the plot is difficult to model because it includes two effects. The first effect is the direct radiation from the rapid temperature rise in the surface of the test panel due to the initial flash. The second effect is the reflected radiation from the walls of the shroud into the camera. This effects disappears when calculating the contrast curve.

The difference of the "water" curve from the "dry" curve is termed the "thermal contrast" curve (shown in Fig. 2 Left). Thermal contrast curves start and end with zero temperature since the initial surface temperature and final equilibrium temperatures are uniform throughout the entire panel. Fig. 2 (Right) shows three contrast curves for three identical water drops behind three different plate thicknesses. It is clear from that figure that the thicker the aluminum plate is the smaller the peak thermal contrast. Fig. 3 (Left) shows four contrast curves for four different quantities of water behind a 1/32" thick aluminum panel. The diameter of the straws was kept constant an equal to ½" while the amount of water was increased. All four curves are very similar in shape and the maximum contrast value. When the experiment was repeated but with thicker aluminum plate, the four contrast curves were very similar again. These results suggest that there is some form of saturation effect when the parameters used for the experiments lay in the range as shown in Table 2. It is important to note that an ideal contrast curve is impossible to achieve since it requires two points on the surface of the panel infinitely apart. Even in a more practical sense it is very difficult to generate systematic contrast curves, because of difficulties in selecting an equivalent reference point on the surface of the panel. Some of the differences seen in Fig. 3 (Left) are simply the result of
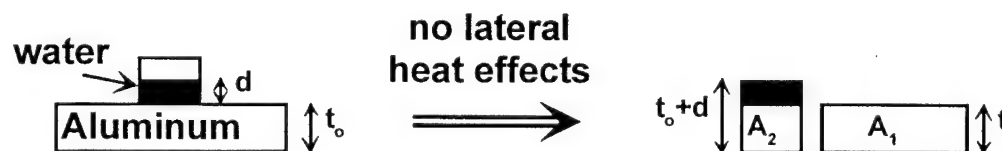

Fig. 4: This Fig. shows a schematic representation of the zero lateral flow assumption used in the model.

difficulties in finding equivalent points over all areas of interest.

Finally Fig. 3 (Right) shows a plot of the maximum thermal contrast as a function of the straw diameter for three aluminum plate thicknesses. Two general observations were noted from this graph. First, water quantity (or height in this case) had negligible effect on contrast and second, thicker aluminum panels resulted in smaller contrast. Each data point on this graph is the average to the peak contrast for the four water contents studied (d=1/16", 1/8", 3/16" and 1/4"). The error bars represent two standard deviations of all peak contrast measurements. In some cases the standard deviations are smaller than the spot used to represent the data point. This again illustrates the fact that for the range of parameters used in this study, the effect of water height was insignificant. We will see later on how our simple model is able to account for this effect. The larger the panel thickness the smaller the contrast. For the thickest aluminum panel (t_o=1/8") only one data point could be obtained due to the small value of the maximum contrast. For the panel with thickness of 1/16" three data points were obtained.

4. CALORIMETRIC MODEL (ZEROTH ORDER APPROXIMATION)

A simple theoretical model (zeroth order approximation) has been derived and it's based on simple calorimetric arguments. Wet and dry regions are defined in this model and it is assumed that no energy flows between them. Fig. 4 shows a schematic representation of the model, where the two regions (dry and wet) have been physically separated to stress that there is no energy flow between them. In the next section a more refined model will be derived that takes into account lateral heat transfer effects.

By using simple calorimetric arguments we can write that $q_1 = \rho_1(A_1 t_o) c_1 T_1$ and $q_2 = \rho_1(A_2 t_o) c_1 T_2 + \rho_2(A_2 d) c_2 T_2$. The parameters q_1, A_1, t_o, ρ_1, and c_1 represent the energy deposited over the area A_1 of an Aluminum panel with thickness t_o density ρ_1 and the specific heat c_1. The parameters q_2, A_2, d, ρ_2, and c_2 represent the energy deposited over the area A_2 of a composite panel made from an aluminum panel of thickness t_o and a layer of water of thickness d, water density ρ_2 and the water specific heat c_2. It was assumed in this model that the initial temperature of the coupon was uniform and equal to zero degrees. Finally, if it is assumed that the energy deposited on the surface of the sample per unit area is constant, i.e., $q_1/A_1 = q_2/A_2 = Q$, then the temperature difference (or thermal contrast) between both blocks $T_1 - T_2 = \Delta T$ will be

$$\Delta T = \frac{Q}{\rho_1 c_1} \frac{1}{t_o} \left(\frac{\rho_2 c_2 \cdot d}{\rho_2 c_2 \cdot d + \rho_1 c_1 \cdot t_o} \right) \qquad (1)$$

This equation correctly describes some of the features of pulsed thermography when applied to this problem.

1. The contrast (ΔT) increases linearly with the amount of energy deposited (Q).
2. The higher the specific heat-density of the substrate ($\rho_1 c_1 \uparrow$) the smaller the peak contrast ($\Delta T \downarrow$)
3. As the water content decreases (d → 0) the contrast vanishes ($\Delta T \to 0$).
4. As the amount of water grows indefinitely (d → ∞) the contrast saturates ($\Delta T \to Q/\rho_1 c_1 t_o$).

It is interesting to note that this simple formula shows a strong dependence of the contrast temperature ΔT on the amount of water "d" inside the straw. As was indicated repeatedly in the previous section, this was not an experimentally observed fact. It is anticipated the lateral heat conduction effect (not included in this model) is responsible for the insensitivity of the contrast temperature ΔT on the variable "d". This assertion becomes obvious if we realize that the thermal conductivity of aluminum is two orders of magnitude larger than that of water. In the next section a simple model that takes into account lateral heat flow effects will be presented.

5. CALORIMETRIC MODEL (FIRST ORDER APPROXIMATION)

In this section the previous model will be modified to allow for lateral heat flow effects. A "poor man's finite element approximation" (i.e. three elements only) will be used. All the elements will be thermally interconnected. Fig. 5 shows a schematic representation of this model. In this model it will be assumed that the in-plane thermal conductivity and the out-of-plane thermal conductivity are different. This will produce the most general results.

In this model it will also be assumed that all the energy of the heat pulse is absorbed in the aluminum plate of thickness "t_o". As a result of this heating process, the temperature "T_o" of the aluminum plate can be derived from $Q = \rho_1 \cdot c_1 \cdot p \cdot T_o$ where it is assumed that the initial temperature of the panel was zero. The quantity K_L represents the lateral thermal conductance while K_{eff} represents the effective out of plane contact thermal conductance. the lateral thermal conductance can be expressed in terms of the lateral thermal conductivity of aluminum k_l (which in this case, since aluminum is isotropic, is just the thermal conductivity of aluminum)

$$K_L = k_l \cdot A_t / R$$
$$K_{eff} = h \cdot A_2$$

(2)

Similarly, the contact conductance can be expressed in terms of an effective contact conductivity "h" between Aluminum and water. A_1 and A_2 are shown in the fig. 5 and represent the surface area of the dry region and the wet region respectively. A_2 can be written as $A_2 = \pi R^2$ where R is the radius of the straw while A_1 will be assumed to tend to infinity ($A_1 \to \infty$). A_t is not shown explicitly in the figure but represents the lateral cross sectional area and can be expressed as $A_t = 2\pi R \cdot t_o$. The set of differential equations that define this problem is

$$\rho_1 \cdot A_1 \cdot t_o \cdot c_1 \cdot \frac{dT_1}{dt} = k_l \cdot \frac{A_t}{R}(T_2 - T_1)$$

$$\rho_1 \cdot A_2 \cdot t_o \cdot c_1 \cdot \frac{dT_2}{dt} = k_l \cdot \frac{A_t}{R}(T_1 - T_2) + h \cdot A_2 \cdot (T_2' - T_2)$$

(3)

$$\rho_2 \cdot A_2 \cdot d \cdot c_2 \cdot \frac{dT_2'}{dt} = h \cdot A_2 (T_2 - T_2')$$

Where T_1, T_2, and T_2' are the temperatures of the different blocks as shown in Fig. 5. This set of coupled differential equations can be written in matrix form as

$$\begin{pmatrix} \dfrac{dT_1}{dt} \\ \dfrac{dT_2}{dt} \\ \dfrac{dT_2'}{dt} \end{pmatrix} = \frac{h}{\rho_1 c_1} \frac{1}{t_o} \begin{pmatrix} -\dfrac{k_l}{h}\dfrac{A_t}{A_1}\dfrac{1}{R} & \dfrac{k_l}{h}\dfrac{A_t}{A_1}\dfrac{1}{R} & 0 \\ \dfrac{k_l}{h}\dfrac{A_t}{A_2}\dfrac{1}{R} & -\dfrac{k_l}{h}\dfrac{A_t}{A_2}\dfrac{1}{R}-1 & 1 \\ 0 & \dfrac{\rho_1 c_1}{\rho_2 c_2}\dfrac{t_o}{d} & -\dfrac{\rho_1 c_1}{\rho_2 c_2}\dfrac{t_o}{d} \end{pmatrix} \begin{pmatrix} T_1 \\ T_2 \\ T_2' \end{pmatrix}$$

(4)

or

$$\frac{d\vec{T}}{dt} = \kappa \cdot \overline{\overline{R}} \cdot \vec{T}$$

(5)

This set of three coupled linear differential equations can be solved by first diagonalizing the matrix $\overline{\overline{R}}$. The second step is to transform the problem into the eigen-space where the equations get de-coupled. In this space the solutions are simple decaying exponential functions, the exponent being related to the eigen-values of the matrix $\overline{\overline{R}}$. Finally the solution in the
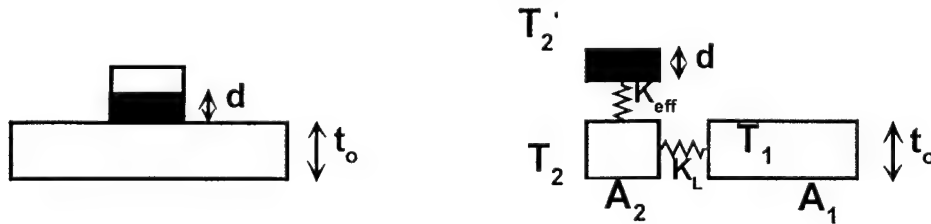

Fig. 5: This figure shows the building blocks of our simple model.

eigen-space has to be transformed back into the original coordinate set. After performing the previous steps and imposing the following boundary conditions

$$T(t = 0) = \begin{pmatrix} T_o \\ T_o \\ 0 \end{pmatrix} \tag{6}$$

where T_o is the initial temperature of the aluminum block (which can be derived from $Q = \rho_1 \cdot c_1 \cdot p \cdot T_o$) the solutions can be obtained and the contrast yields

$$\Delta T(t) = \frac{Q}{\rho_1 c_1 \cdot t_o \cdot \sqrt{(1+a+r)^2 - 4ar}} \left(e^{-\frac{h}{\rho_1 c_1} \frac{\lambda_1}{t_o} t} - e^{-\frac{h}{\rho_1 c_1} \frac{\lambda_2}{t_o} t} \right) \tag{7}$$

where $a = \dfrac{k_L}{h} \dfrac{A_t}{A_2} \dfrac{1}{R}$ and $r = \dfrac{\rho_1 c_1}{\rho_2 c_2} \dfrac{t_o}{d}$ (don't confuse the variable "t = time" with the parameter "t_o = panel thickness").

The parameters λ_1 and λ_2 are the non-trivial eigen-values of the matrix $\overline{\overline{R}}$ defined above.

The maximum or peak thermal contrast can be calculated by differentiating Eq. 7 and the result gives

$$\Delta T_{peak} = \frac{Q}{\rho_1 c_1} \frac{2}{t_o(1+a+r+\sqrt{(1+a+r)^2 - 4ar})} \cdot \left[\frac{1+a+r-\sqrt{(1+a+r)^2 - 4ar}}{1+a+r+\sqrt{(1+a+r)^2 - 4ar}} \right]^{\frac{1+a+r-\sqrt{(1+a+r)^2-4ar}}{2\sqrt{(1+a+r)^2-4ar}}} \tag{8}$$

which happens at a time give by

$$t_{peak} = \frac{\rho_1 c_1}{h} \frac{t_o}{\sqrt{(1+a+r)^2 - 4ar}} \ln\left(\frac{1+a+r+\sqrt{(1+a+r)^2 - 4ar}}{1+a+r-\sqrt{(1+a+r)^2 - 4ar}} \right) \tag{9}$$

It can be shown that in the limit when the lateral heat flow effects disappear, i.e $k_L \to 0$ (or $a \to 0$) then Eq. 8 reduces to Eq. 1 as it would be expected. In practice the contact conductivity "h" is much smaller that the lateral thermal conductivity of aluminum "k_l", as a result a >> r > 1. If eqs. 7, 8 and 9 are expanded around "a" in this limit, it can be shown that

$$\Delta T(t) = \frac{Q}{\rho_1 c_1 \cdot t_o \cdot a} \left(e^{-\frac{h}{\rho_2 c_2} \frac{1}{d} t} - e^{-\frac{k_l}{\rho_1 c_1} \frac{1}{R^2} t} \right) \tag{10}$$

$$\Delta T_{peak} = \frac{Q}{\rho_1 c_1} \frac{1}{a \cdot t_o} \cdot \left[\frac{r}{a} \right]^{\frac{r}{a}} \tag{11}$$

and finally

$$t_{peak} = \frac{\rho_1 c_1}{h} \frac{t_o}{a} \ln\left(\frac{a}{r} \right) \tag{12}$$

It is important to stress that the previous three equations were derived in the limit a >> r, which happens to be the "material parameter space" region considered in this work as shown in Table 1. As an example, a vanishing amount of water in a straw, i.e. when d << t_o, would not fall within these "material parameter space" region and therefore would not be properly modeled by the previous equations. A desirable property of eq. 11 is that it depends very weakly on the variable "d". This

weak dependence on "d" was experimentally observed and was described in section 3. The variable "d" only enters into eq. 11 via the parameter "r". If "r" << "a" then $(r/a)^{r/a} \to 1$ and ΔT actually becomes an independent function of "d".

6. ANALYSIS OF RESULTS

Figure 6 (left) shows all experimental data points and the fit to them using eq. 11. It can be seen from the graph that this simple model fits the experimental results fairly well. The largest fitting discrepancies happen for the panel with thickness 1/32". Figure 6 (right) shows the ½" straw diameter data curves for three different panel thickness and a fit to them using eq. 11. It can be seen again that the fitting results for the 1/32" thick panel show the largest discrepancies. The starting parameters that were used for all these fits

Aluminum 7075 T6	Water
$\rho_1 = 2.8$ g/cm^3	$\rho_2 = 1$ g/cm^3
$c_2 = 0.84$ J/(g K)	$c_2 = 4.1$ J/(g K)
$k_1 = 1.29$ W/(cm K)	$h = 8.2$ mW/(cm^2 K)

Table 2: Relevant material property values

are shown in table 2 and were obtained from standard material properties handbooks except for the contact conductivity. The final fitting values were found to be reasonably close to these starting parameters. The starting value for the contact conductivity was chosen to be the thermal conductivity of water per unit centimeter. The final fitting value was found to be significantly larger than this initial estimate.

It is important to emphasize some of the problems found when dealing with the type of data described in this paper and when using this simple model. The first problem that one is faced with is in generating the contrast curves. As was mentioned in section three, and ideal contrast curve should be generated by subtracting a reference curve taken far away from any region of the panel that has water from a curve taken under a region with water. This requirement was difficult to meet because of the finite size of our sample and because of the many regions with water that we had in our panel. To overcome this difficulty one could use one aluminum panel for each water drop geometry. The problem with this approach would be that a large number of panels would be require and non-systematic errors would be introduced to the data such as room temperature variations and varying amounts of heat deposited onto the surface of the sample. Another source of random errors was the straw fabrication. Straws were not perfectly circular and the diameter as a result had random errors.

The model used in this work makes some drastic approximations such as; 1) a very small number of blocks with average temperatures to describe the transient behavior of the system, 2) temperature independent material properties, 3) no cooling effects introduced through radiation, 4) uniform initial temperature distribution, 5) single drop on panel (as opposed the multitude of drops actually used in the panels), 6) transverse conductivity approximated by a contact conductance and 7) does not take into account the thermal properties of the straw. It is anticipated that many refinements to the model can be achieved by improving on some of the approximations. Despite its crudeness the model is robust enough to fit the experimental data accurately enough.
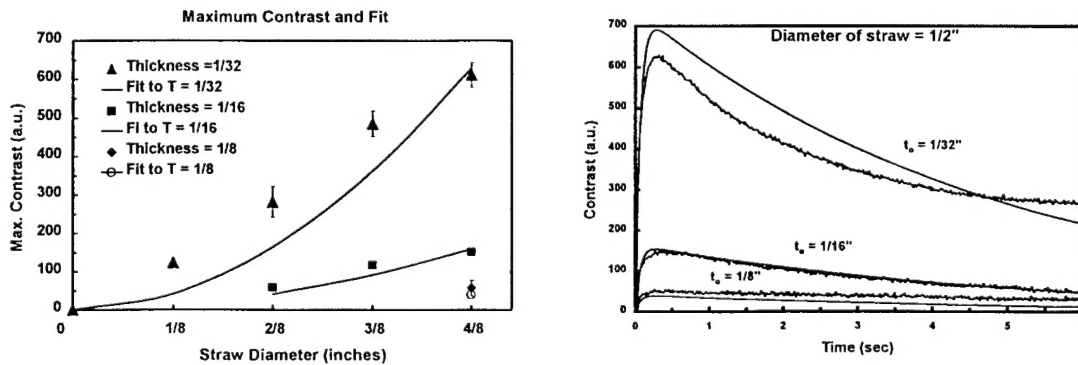

Fig. 6: This figure shows a fit (solid lines) using eqs. 8 or 11 to the experimental contrast data for three different plate thicknesses. The error bars represent the range in peak contrast temperatures for the various amounts of water used in the experiments.

7. CONCLUSION

Two simple models have been developed (figs. 4 and 5) that to a first order approximation describes the main features of thermal pulse analysis when applied to a planar flaw. The first model, zeroth order approximation does not take into account lateral heat conduction effects. The second model takes into account lateral heat conduction effects, thickness effects, water size effects, density effects, thermal transients. The model correctly predicts the relationships between the previous parameters. Eqs. 7, 8 and 9 are the main output of the mode or their expansions around he parameter "a" (eqs. 10, 11 and 12) . This relations were shown to model correctly the time dependence of the thermal contrast, the peak thermal contrast and the time at which the thermal contrast peaks.

8. ACKNOWLEDGEMENTS

9. REFERENCES

1 R. Wegman, *Nondestructive Test Methods for Structural Composite*, SAMPE Handbook No. 1, SAMPE International Business Office, Covina, CA, 1989, pp13-26

2 I. Perez, P. Kulowitch and S. Shepard, "Modeling of pulsed thermography in anisotropic media". Proceedings of the 25th Annual Progress in QNDE, Snowbird Colrado, July 19-24, 1998

3 I. Perez, R. Santos, P. Kulowitch and M. Ryan. "Calorimetric Modeling of Thermographic Data". Proceedings of SPIE Conference, Thermosense XX,. J.R. Snell, Jr. and R.N. Wurzbach Eds., 14-16 April 1998, pp75-83

REPORT DOCUMENTATION PAGE

1. REPORT DATE *2000*	2. REPORT TYPE Professional Paper	3. DATES COVERED
4. TITLE AND SUBTITLE Thermography for the Characterization of Corrosion Damage		5a. CONTRACT NUMBER
		5b. GRANT NUMBER
		5c. PROGRAM ELEMENT NUMBER
6. AUTHOR(S) Ignacio Perez Paul Kulowitch		5d. PROJECT NUMBER
		5e. TASK NUMBER
		5f. WORK UNIT NUMBER
7. PERFORMING ORGANIZATION NAME(S) AND ADDRESS(ES) Naval Air Warfare Center Aircraft Division 22347 Cedar Point Road, Unit #6 Patuxent River, Maryland 20670-1161		8. PERFORMING ORGANIZATION REPORT NUMBER
9. SPONSORING/MONITORING AGENCY NAME(S) AND ADDRESS(ES) Naval Air Systems Command 47123 Buse Road Unit IPT Patuxent River, Maryland 20670-1547		10. SPONSOR/MONITOR'S ACRONYM(S)
		11. SPONSOR/MONITOR'S REPORT NUMBER(S)

12. DISTRIBUTION/AVAILABILITY STATEMENT

Approved for public release; distribution is unlimited.

13. SUPPLEMENTARY NOTES

14. ABSTRACT

Thermography is a viable NDE technique for the characterization of corrosion in metallic materials. Thermography is a rapid, noncontact, wide area inspection technique that is easy to interpret and that is not significantly sensitive to material curvature. We have developed a portable system and have characterized the sensitivity of the technique. Results will be presented in this paper.

15. SUBJECT TERMS

Thermography, thermographic inspection, corrosion, naval aviation, corrosive environment, lateral heat effects

16. SECURITY CLASSIFICATION OF:			17. LIMITATION OF ABSTRACT	18. NUMBER OF PAGES	19a. NAME OF RESPONSIBLE PERSON Ignacio Perez
a. REPORT	b. ABSTRACT	c. THIS PAGE			19b. TELEPHONE NUMBER (include area code)
Unclassified	Unclassified	Unclassified	Unclassified	35	(301) 342-8074